P 2 min

(NASA-CR-137C77) DYNAMIC EVALUATION OF RPI'S 0.4 SCALE UNMANNED MARTIAN ROVING VEHICLE MODEL M.S. Thesis (Rensselaer Polytechnic Inst.) 57 p HC $6.00

N74-17957

CSCL 13F G3/11

Unclas

16725

R.P.I. TECHNICAL REPORT MP-38

DYNAMIC EVALUATION OF RPI'S 0.4 SCALE UNMANNED MARTIAN ROVING VEHICLE MODEL

by

Alan G. Ryder

National Aeronautics
and Space Administration

Grant NGL 33-018-091

A project submitted to the Graduate
Faculty of Rensselaer Polytechnic Institute
in partial fulfillment of the
requirements for the degree of

MASTER OF ENGINEERING

School of Engineering
Rensselaer Polytechnic Institute
December 1973

CONTENTS

ABSTRACT

A design for a Mars Roving Vehicle has been underway at Rensselaer Polytechnic Institute for the past four years. The basic configuration has been developed. It now remains to design and develop the deployment mechanisms, and then to optimize the total design.

A basic mathematical model of the vehicle is a valuable tool in the optimization of the design. This project report presents such a three dimensional model considering three degrees of freedom. In addition, the physical characteristics of the 0.4 scale RPI-MRV are presented along with the basic dynamic responses.

LIST OF FIGURES

LIST OF PLATES

ACKNOWLEDGEMENTS

The work reported in this paper was sponsored under N.A.S.A. project-contract NGL 33-018-091. The project is administered at Rensselaer Polytechnic Institute by Dr. Stephen Yerazunis, Associate Dean of the School of Engineering.

Dr. George N. Sandor, Chairman of the Machines and Structures Division, and the project Vehicle Group advisor, has provided much guidance. John Almstead, student group leader, was most helpful throughout the duration of the work. Don Shaver provided much technical and shop assistance.

Finally, a special thanks goes to Dr. Czeslaw A. Broniarek, Assistant Professor of Mechanical Engineering, who provided the motivation and theoretical assistance.

CHAPTER 1

INTRODUCTION

Although the major point of emphasis of today's outer space program has been shifted during the past year or two, the intriguing question of the possibility of some form of life on the planet Mars remains. A NASA unmanned mission to our Earth's nearest neighbor is currently planned for approximately the 1980 time frame. The basic objective of the mission is to deploy scientific packages and to conduct scientific experiments.

It was learned from the Viking Mission that the useful capability of a stationary lander is severely limited. Because of topographic requirements, a landing site is not necessarily the most interesting from a scientific viewpoint. In addition, because of the terrain disturbance caused by the landing maneuver, it is desirable to conduct scientific explorations in undisturbed areas remote from the landing site. Therefore, it is desirable to place a mobile package on the surface of Mars. For this purpose, RPI's Martian Roving Vehicle (MRV) is being developed (Plate 1).

A current NASA sponsored project has as its objective the design and development of the complete MRV including the locomotion and navigation systems. The subject of this paper is the dynamic analysis of the RPI design of the MRV.

The dynamic analysis of the MRV was approached by two methods:

(1) mathematical modeling

(2) physical testing

Initially the equations of motion of a three dimensional, three-degree -of-freedom (roll,pitch,vertical displacement) model are established. Then, the measurement of the physical characteristics of the 0.4 MRV model and dynamic tests were conducted. Finally, a

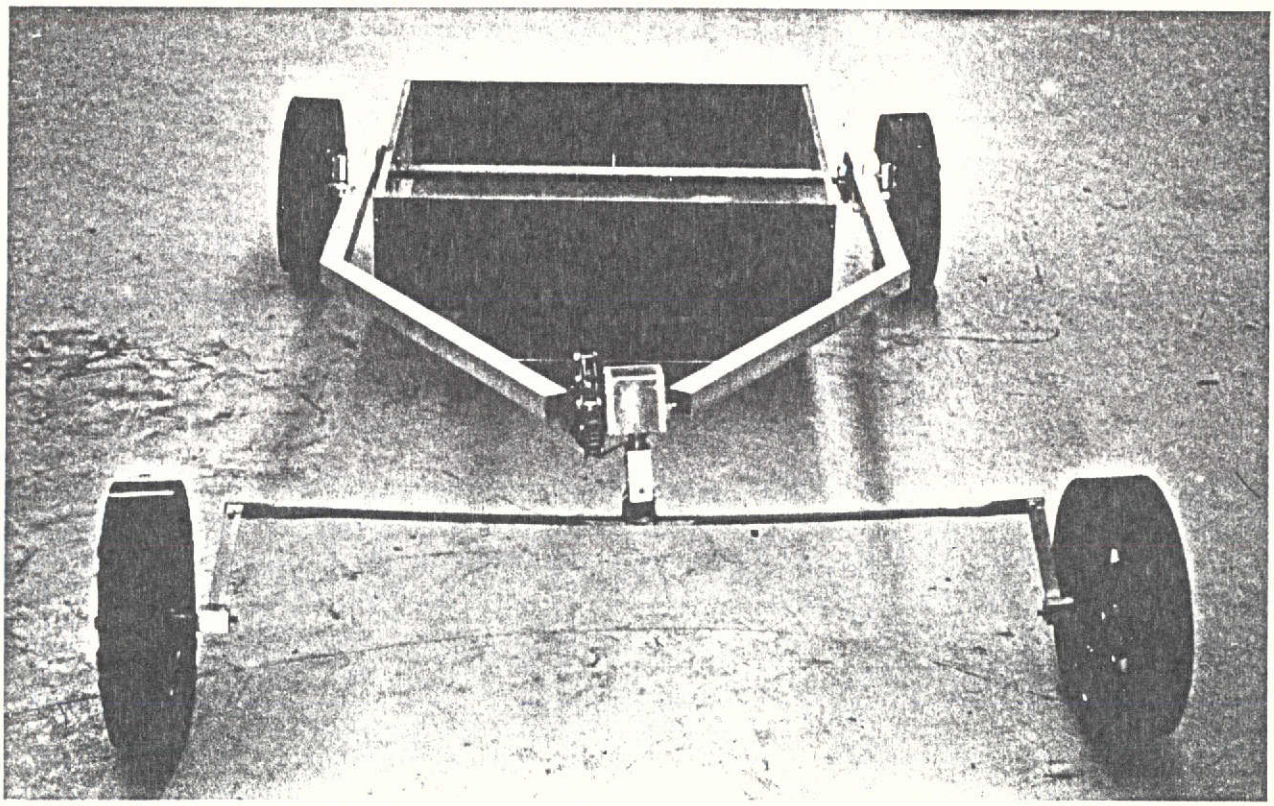

PLATE 1

RPI-MRV 0.4 Scale Model

comparison of actual response with the mathematically predicted response is made. The result shows the mathematical model to be a basic design tool from which gross vehicle motions may be predicted. It also may be expanded upon to develop a more sophisticated mathematical model.

CHAPTER 2

THE MATHEMATICAL MODEL

The 0.4 scale model of the RPI-MRV is shown in Plate 1. Elasticity and damping in the suspension of the vehicle is provided almost entirely by the all metal, toroidal, elastic wheel. The rear wheel struts are connected to a torsion bar, and the front wheels are attached to a flexible front axle. Since the stiffness of the rear torsion bar and the front axle is much greater in comparison to the wheel stiffness, only the wheel elasticity is considered in the mathematical model presented herein. Figure 1 shows the schematic model. The wheels have been replaced by springs and dashpots. This is the schematic from which the mathematical model is developed.

In the development of an initial approach, a highly useable mathematical model is the primary objective. Since coupling between modes of motion does exist and is a problem in the physical model, the idea of a planar mathematical model was discarded in favor of one considering three dimensions.

Again for simplicity, three degrees of freedom are considered. Vertical displacement is an obvious choice since the MRV bouncing across Martian terrain will be carrying a scientific payload. Because of the "dragster" design of the RPI-MRV, the vehicle center of gravity is located near the rear wheel base far from the center of suspension. A natural pitching motion is therefore introduced by the vehicle design. As a result, the mathematical model also includes pitch motion. Finally, the movement of the MRV over rocks

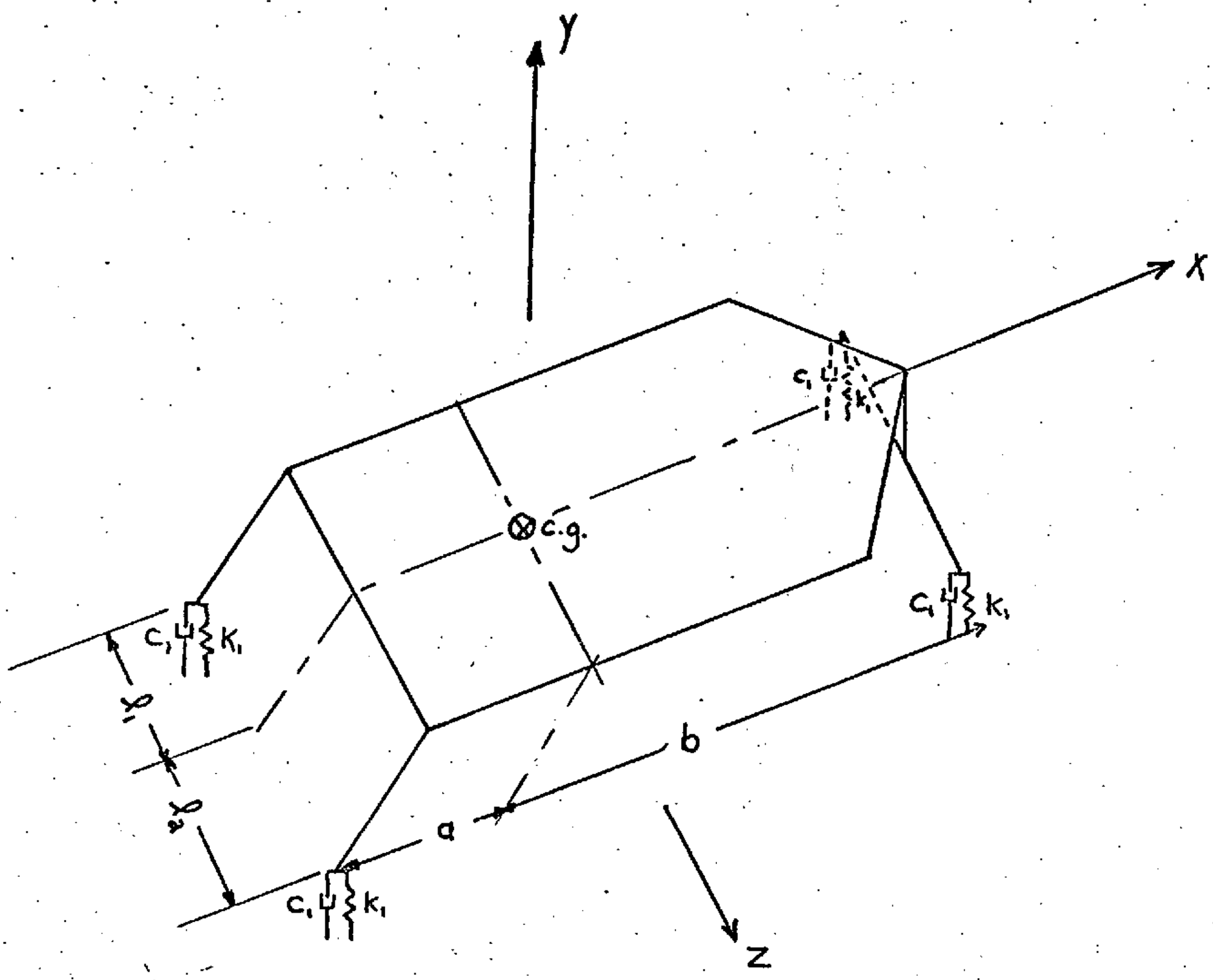

FIGURE 1

RPI-MRV Schematic Model

and potholes easily introduces a rolling motion. Therefore, with the three degrees of freedom chosen to be vertical displacement, roll, and pitch rotation, the development of the equations of motion proceeded.

<u>The Inertia Forces</u>.

In order to greatly simplify the equations of motion, the MRV is considered to be a two-mass system: a rolling (sprung) mass, and a non-rolling (unsprung) or fixed mass. Additionally, if a moving coordinate system, x'y'z' fixed to the vehicle is adopted, the inertial terms in the equations of motion become much easier to determine. Therefore, the coordinate system of Figure 2 is used. The xyz axis system is fixed to the unsprung portion of the vehicle.

The vertical y axis is located by the c.g. of the complete vehicle which, for the MRV, is approximated by the location of the rolling mass (since $m_r \gg m_u$). The x axis is the roll axis of the vehicle, located by the kinematic properties of the suspension. The unsprung mass is assumed to be located on this axis. The origin of the x'y'z' axes coincides with the sprung (rolling) mass.

The inertia forces written about the x'y'z' axes are as follows:

$$\begin{aligned}
\Sigma F_{y'} &= m_r \ddot{y}' \\
\Sigma M_{x'} &= I_{x'x'}\dot{\omega}_{x'} + I_{x'y'}(-\omega_{z'}\omega_{x'}) + I_{x'z'}\dot{\omega}_{z'} + I_{y'z'}(-\omega_{z'}^2) \\
\Sigma M_{z'} &= I_{z'z'}\dot{\omega}_{z'} + I_{z'x'}\dot{\omega}_{x'} + I_{z'y'}(\omega_{x'}\omega_{z'}) + I_{x'y'}(\omega_{x'}^2)
\end{aligned} \tag{1}$$

Assuming: (1) Near symmetry in the x'z' plane, $I_{x'z'}=0$

(2) $I_{y'z} \ll I_{x'y'}$

(3) $I_{x'y'}=I_{xy} \approx 0$ since the y axis is chosen through the c.g.

equations (1) become:

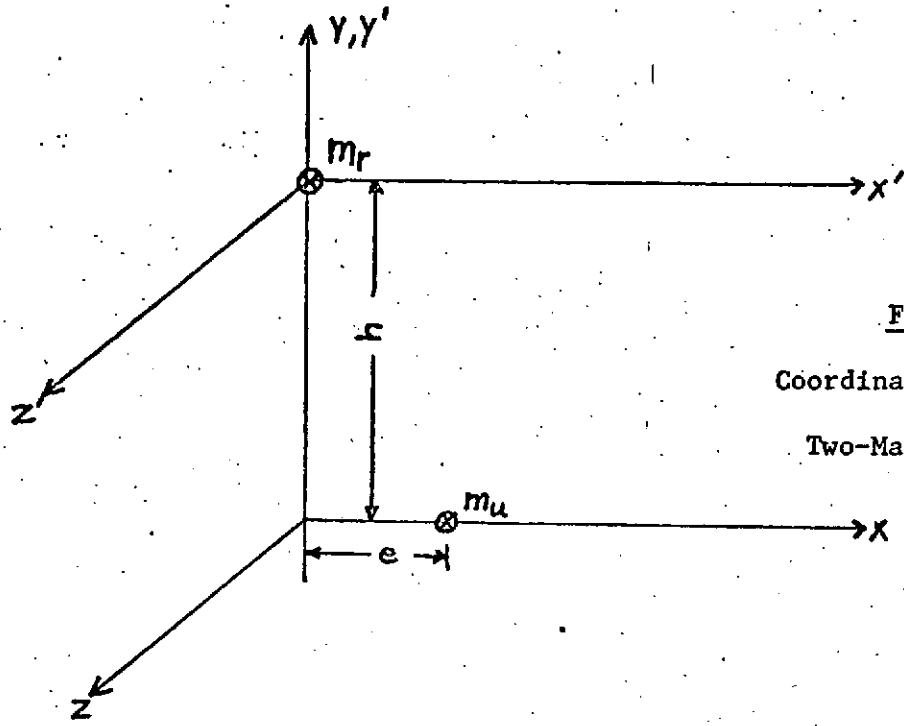

FIGURE 2

Coordinate System of

Two-Mass Vehicle

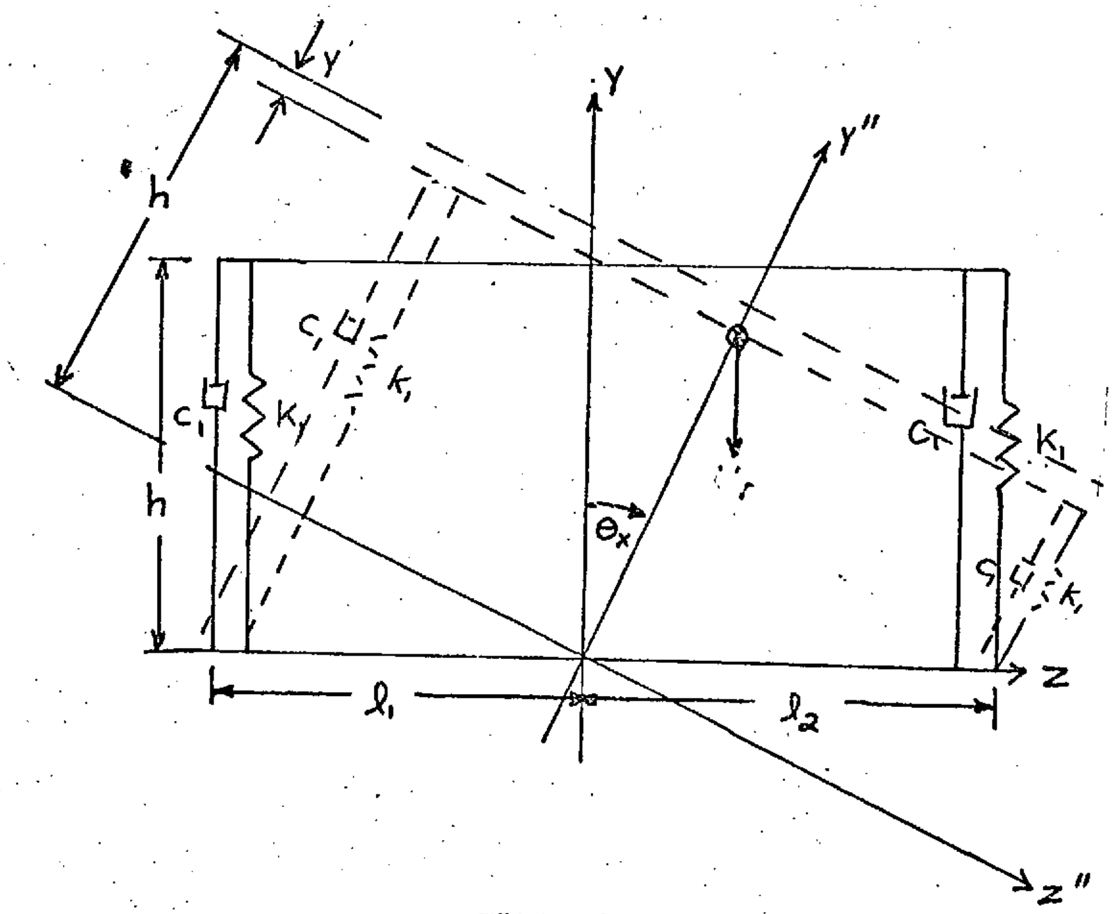

FIGURE 3

Roll (θ_x) with Vertical Displacement (y)

$$\Sigma F_{y'} = m_r \ddot{y}'$$
$$\Sigma M_{x'} = I_{x'x'} (\dot{\omega}_{x'}) \qquad (2)$$
$$\Sigma M_{z'} = I_{z'z'} (\dot{\omega}_{z'})$$

For small displacements, the roll and pitch velocities about the inclined x'y'z' axes will be respectively equal to the roll and pitch velocities about the xyz axes (i.e. $\omega_{x'} = \omega_x, \omega_{z'} = \omega_z$). This approximation along with the following expressions:

$$I_{xx} = I_{x'x'} + m_r h^2$$
$$I_{zz} = I_{z'z'} + m_r h^2$$

enable equations (2) to be translated to the xyz axes:

$$\Sigma F_y = m_r \ddot{y}$$
$$\Sigma M_x = I_{xx} \dot{\omega}_x \qquad (3)$$
$$\Sigma M_z = I_{zz} \dot{\omega}_z$$

With a change of notation using

$$\dot{\theta}_x = \omega_x$$
$$\dot{\theta}_z = \omega_z \qquad (4)$$

The final inertia forces take the form:

$$\Sigma F_y = m_r \ddot{y}$$
$$\Sigma M_x = I_{xx} \ddot{\theta}_x \qquad (5)$$
$$\Sigma M_z = I_{zz} \ddot{\theta}_z$$

The External Forces.

The weight of the sprung mass merely causes a steady static deflection of the wheels about which the dynamic oscillations take place. Therefore the external forces of the idealized schematic model result wholly from the spring and damping forces of the wheel. These forces are considered linear. As indicated later, this assumption proves to be valid.

To determine the external forces and moments, the vehicle model assumes two sets of virtual displacements:

(1) roll with vertical displacement

(2) pitch with vertical displacement

Assuming a roll with vertical displacement (Figure 3), the vertical forces become:

$$F_y = -(k_1 + c_1 s)(y - \ell_1\theta_x) - (k_1 + c_1 s)(y + \ell_2\theta_x) - (k_1 + c_1 s)2y \tag{6}$$

where s denotes the operator $\frac{d(\,)}{dt}$. The displacement of the front wheel axle is independent of the roll angle displacement because of the pin-joint connection between the frame and the front axle. This accounts for the last term in equation (6) not being dependent upon θ_x. The moments resulting from the displacement of Figure (3) are:

$$M_x = (\ell_1 - h\theta_x)(k_1 + c_1 s)(y - \ell_1\theta_x) - (\ell_2 + h\theta_x)(k_1 + c_1 s)(y + \ell_2\theta_x) + w_r(h - y)\theta_x \tag{7}$$

Again, as a result of the pin-joint mentioned above, the front suspension imparts no rolling motion to the vehicle. Using the small displacement approximations, $\ell_1 \gg h\theta_x$, $\ell_2 \gg h\theta_x$, and, $h \gg y$, equations (6) and (7) become:

$$F_y = -(k_1 + c_1 s)\left[(y - \ell_1\theta_x) + (y + \ell_2\theta_x) + 2y\right] \tag{8}$$

$$M_x = (k_1 + c_1 s)\left[y(\ell_1 - \ell_2) - \theta_x(\ell_1^2 + \ell_2^2)\right] + w_r h\theta_x \tag{9}$$

Figure 4 shows a pitch angle with vertical displacement. The

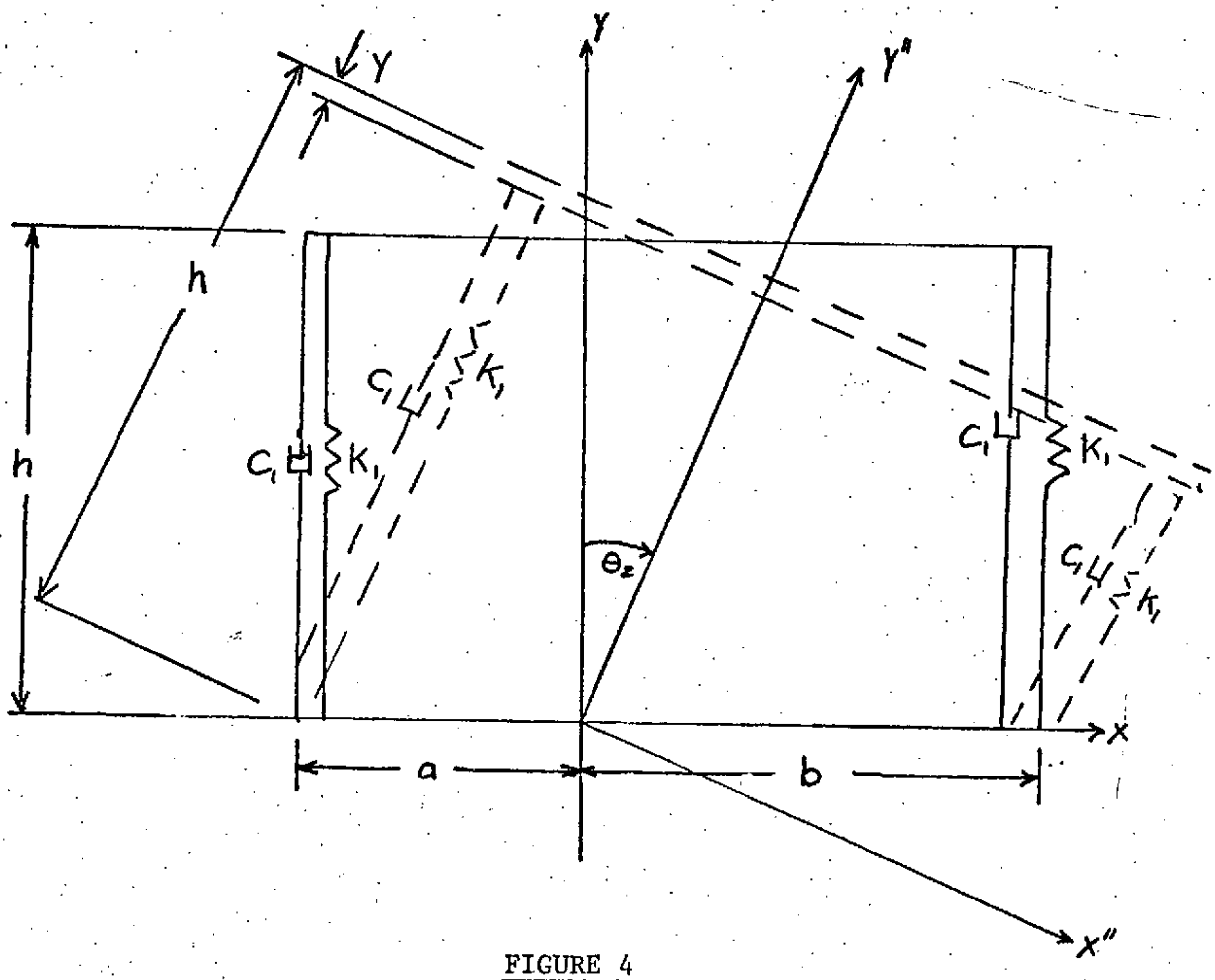

FIGURE 4

Pitch (θ_z) with Vertical Displacement (y) resulting force and moment equations become:

$$F_y = -2(k_1+c_1 s)\left[(y-a\theta_z)+(y+b\theta_z)\right] \tag{10}$$

$$M_z = 2(k_1+c_1 s)\left[(a-h\theta_z)(y-a\theta_z)-(b+h\theta_z)(y+b\theta_z)\right] + w_r(h-y)\theta_z \tag{11}$$

Again with the small displacement approximations, $b \gg h\theta_z$, $a \gg h\theta_z$, equations (10) and (11) simplify to:

$$F_y = -2(k_1+c_1 s)\left[2y+(b-a)\theta_z\right] \tag{12}$$

$$M_z = 2(k_1+c_1 s)\left[y(a-b)-\theta_z(a^2+b^2)\right] + w_r h\theta_z \tag{13}$$

<u>The Complete Equations</u>.

The complete equations of motion for the three-dimensional, three-degree -of-freedom model result from the combination of equations (5),(8),(9),(12), and (13):

$$\begin{aligned} m_r\ddot{y} &= -(k_1+c_1 s)\left[(y-\ell_1\theta_x)+(y+\ell_2\theta_x)+2\theta_z(b-a)+4y\right] \\ I_{xx}\ddot{\theta}_x &= (k_1+c_1 s)\left[y(\ell_1-\ell_2)-\theta_x(\ell_1^2+\ell_2^2)\right]+w_r h\theta_x \\ I_{zz}\ddot{\theta}_z &= 2(k_1+c_1 s)\left[y(a-b)-\theta_z(a^2+b^2)\right]+w_r h\theta_z \end{aligned} \tag{14}$$

These equations may be simplified as follows:

$$\begin{aligned} &\ddot{y}+a_{11}\dot{y}+a_{12}y+b_{11}\dot{\theta}_x+b_{12}\theta_x+c_{11}\dot{\theta}_z+c_{12}\theta_z=0 \\ &\ddot{\theta}_x+b_{21}\dot{\theta}_x+b_{22}\theta_x+a_{21}\dot{y}+a_{22}y=0 \\ &\ddot{\theta}_z+c_{31}\dot{\theta}_z+c_{32}\theta_z+a_{31}\dot{y}+a_{32}y=0 \end{aligned} \tag{15}$$

where

$a_{11}=-4c_1/m_r$ $\quad$ $b_{11}=(\ell_2-\ell_1)c_1/m_r$

$a_{12}=-4k_1/m_r$ $\quad$ $b_{12}=(\ell_2-\ell_1)k_1/m_r$

$a_{21}=(\ell_2-\ell_1)c_1/I_{xx}$ $\quad$ $b_{21}=(\ell_1^2+\ell_2^2)c_1/I_{xx}$

$a_{22}=(\ell_2-\ell_1)k_1/I_{xx}$ $\quad$ $b_{22}=(\ell_1^2+\ell_2^2)k_1/I_{xx}-w_r h/I_{xx}$

$a_{31}=2(b-a)c_1/I_{zz}$

$a_{32}=2(b-a)k_1/I_{zz}$

$$c_{11}=2(a-b)c_1/m_r$$
$$c_{12}=2(a-b)k_1/m_r$$
$$c_{31}=2(a^2+b^2)c_1/Izz$$
$$c_{32}=2(a^2+b^2)k_1/I_{zz}-w_r h/I_{zz}$$

Equations (15) are a set of second order linear differential equations to be solved simultaneously. A digital computer program titled DYNAMO (from DYNAmic MOdels) was used to solve equations (15). Appendix A is a listing of the program used.

Various terrain conditions may be simulated on the mathematical model. A step input to the vehicle c.g. is simulated by assuming an initial condition on the vertical displacement. An initial condition on pitch displacement simulates a step either to the front or rear wheel pair as would be encountered by the vehicle's front wheels hitting a sudden difference in elevation. Similarly an initial condition on roll displacement simulates a step to either the right or left side wheel pair. A washboard terrain effect can be modeled by equating the left side of the first of equations (15) to a sinusoidal forcing function of desired frequency and amplitude. The c.g. response to various terrains may be simulated by equating the left side of the proper equation of equation (15) to the appropriate function.

This mathematical model may easily be extended to:

(1) include a spring and damper to be located in the connection of the frame to the front axle, or

(2) to consider wheels of different elastic properties.

Appendices B and C list the resulting equations of motion. This model may also be extended to include additional degrees of freedom.

Specifically, because of a lateral stiffness problem with the all metal toroidal wheel, the additional degrees of freedom of lateral translational and yaw displacements may be useful extensions.

CHAPTER 3

MEASUREMENT OF THE 0.4 RPI-MRV PHYSICAL CHARACTERISTICS

Once the equations of motion were developed, the physical characteristics of the 0.4 scale model MRV were determined in order to convert the equations of motion into meaningful results. Most of the measurements were determined in a straightforward manner. The sprung, unsprung, and total vehicle mass (earth-weight), and the dimensions locating the vehicle center of gravity are listed in Plate 2. The remaining characteristics proved to be more difficult to measure, and are discussed below.

Spring Constant. The sole source of flexibility considered in the mathematical model was the all-metal wheel. All four wheels were tested with the apparatus shown in Plate 3. The force-deflection curve of figure 5 shows the results. The spring proves to be quite linear with a spring constant of k_1=34.5 lb_f/in. As discussed later, the actual dynamics of the MRV were measured with a capacitance-displacement measurement system, capable of measuring displacements of under one inch. To protect the capacitance probes, displacements were limited to a maximum amplitude of 1/4 inch. Under such small loads yielding small deflections, the spring constant of the wheel was found to be lower than the large-load spring constant. Figure 6 shows the wheel deflection characteristic under small loads, indicating a spring constant of k_1=24.8 lb_f/in.

Damping Coefficient. The damping coefficient of the wheel, associ-

Summary of 0.4 Scale RPI-MRV Physical Characteristics

Vehicle

Total earth weight	$w=51.0\ lb_f$
Total mass	$m=1.58$ slugs
Front wheel load	$7.5\ lb_f$/wheel
Rear wheel load	$18\ lb_f$/wheel
Sprung earth weight	$w_r=49.0\ lb_f$
Sprung mass	$m_r=1.52$ slugs
Unsprung earth weight	$w_u=2.0\ lb_f$
Unsprung mass	$m_u=0.06$ slugs

Dimensions: (see Figures 1 and 9)

$\ell_1=21.0$ in

$\ell_2=23.0$ in

a=22-1/4 in

b=34-3/4 in

h=10.0 in

Moments of inertia of rolling mass (m_r) (see Figure 2)

$I_{x'x'}=2.73$ slug-ft^2	$I_{xx}=3.73$ slug-ft^2
$I_{y'y'}=6.30$ slug-ft^2	$I_{yy}=6.30$ slug-ft^2
$I_{z'z'}=5.67$ slug-ft^2	$I_{zz}=6.67$ slug-ft^2

Wheel

Spring constant $k_1=414\ lb_f/ft$ (large loads)

$k_1=298\ lb_f/ft$ (small loads, see discussion)

Damping coefficient $C_1=4.0\ lb_f/ft/sec$

PLATE 2

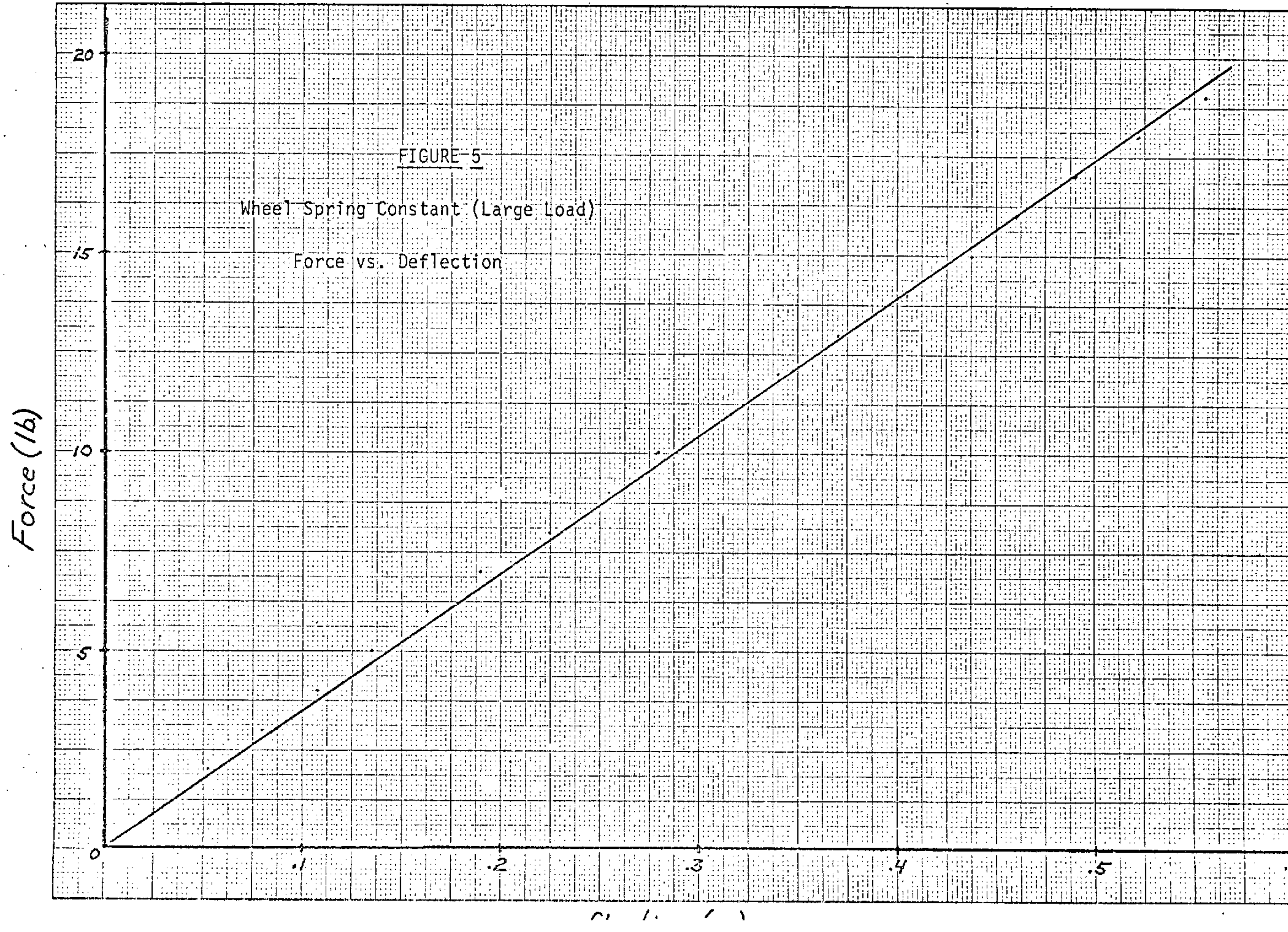
FIGURE 5
Wheel Spring Constant (Large Load)
Force vs. Deflection
Force (lb)
20
15
10
5
0
.1
.2
.3
.4
.5
.6

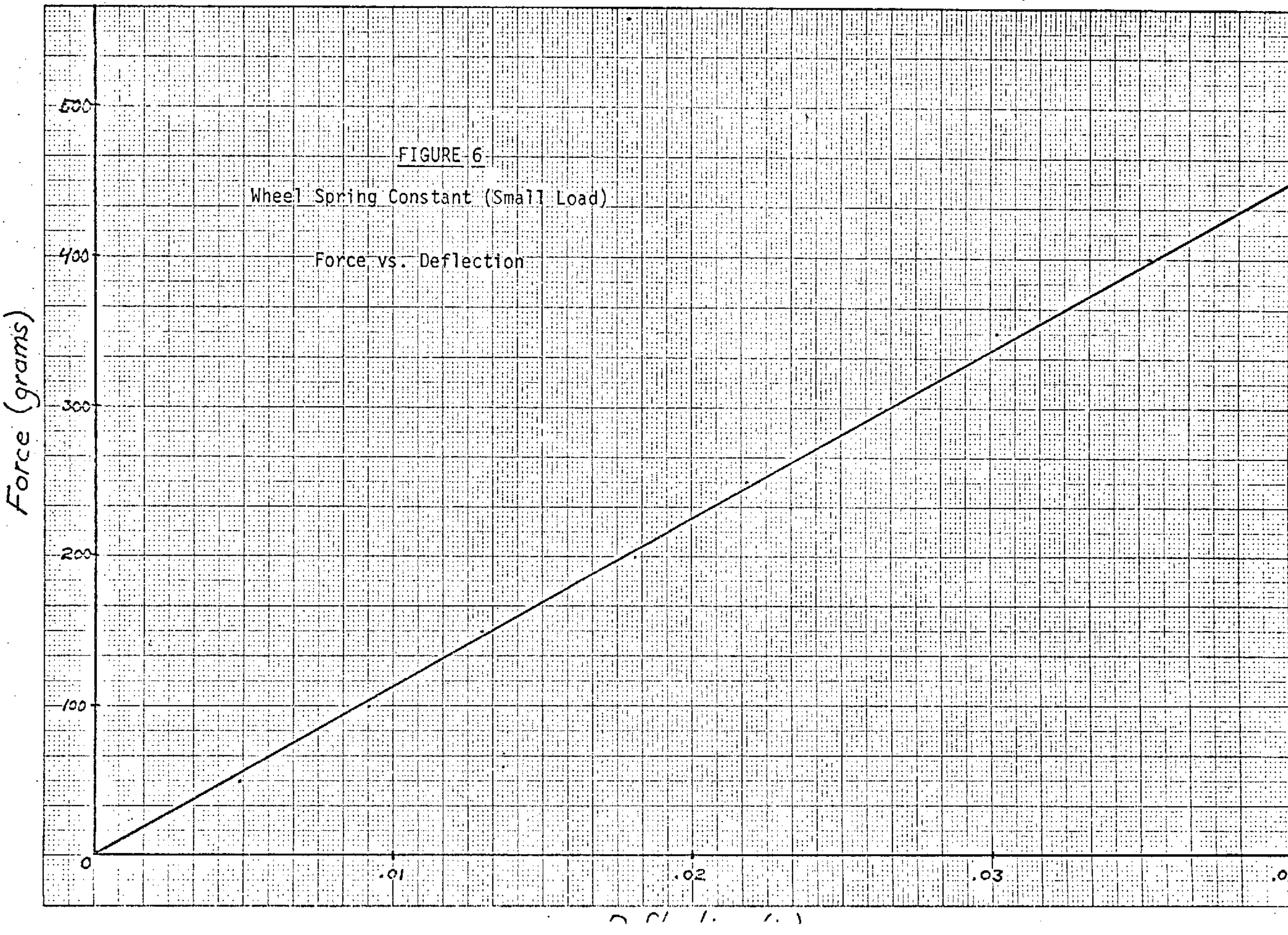
FIGURE 6
Wheel Spring Constant (Small Load)
Force vs. Deflection
Force (grams)
500
400
300
200
100
0
.01
.02
.03
.04

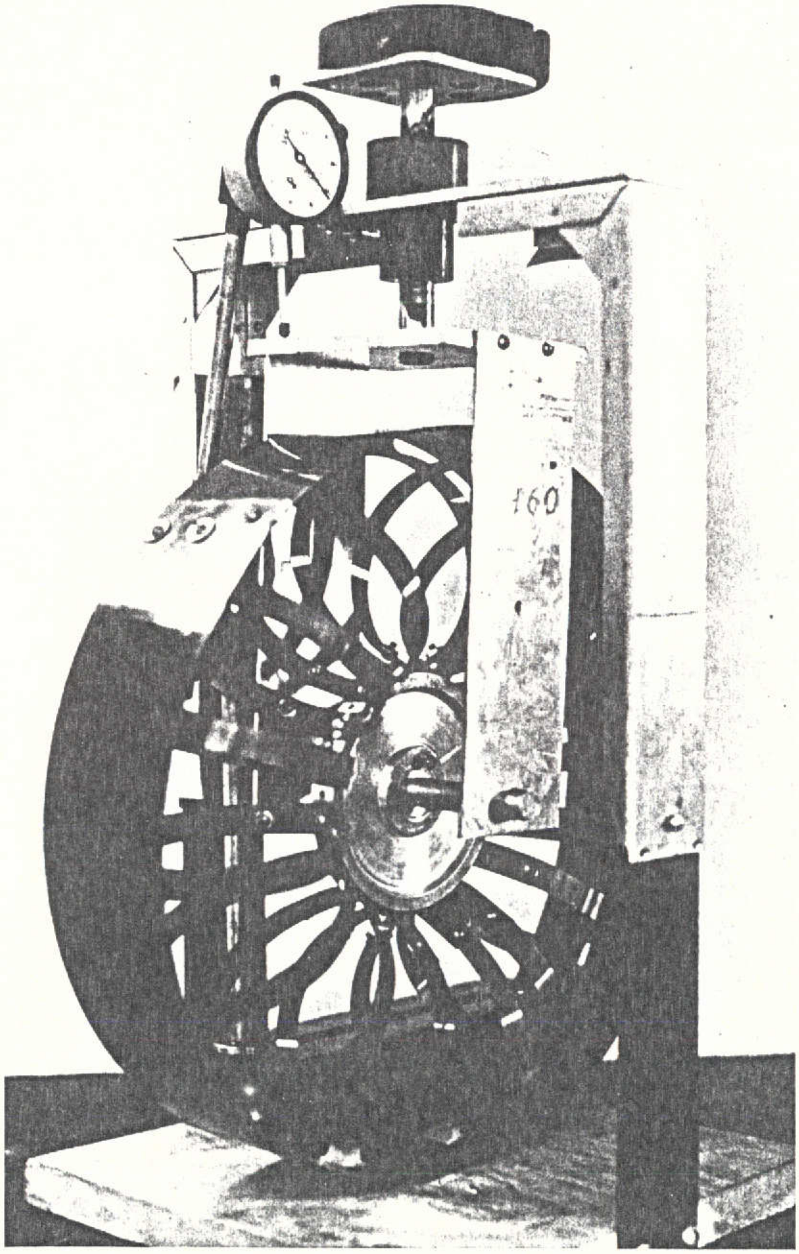

PLATE 3

Wheel Spring and Damping Tester

ted with the spring, was more difficult to determine. The apparatus shown in plate 3 was used. Several tests were conducted in order to find a few tests during which the wheel was allowed to vibrate freely. The capacitance displacement measuring equipment was used to monitor the motion. A strip chart recorder was used to gain a time displacement plot (figure 7). In order to decrease the period of oscillation, and therefore increase accuracy, the tests were conducted with the wheel axle loaded to 8 pounds. The critical damping coefficient C_c is easily determined from

$$C_c=2m\sqrt{k/m}$$

The logarithmic decrement (δ) of vibration decay is determined by measuring the amplitude of successive peaks of vibration (figure 7) and the following expression

$$\delta=\ln(x_n/x_{n+1})$$

The logarithmic decrement can then be related to the damping ratio (ρ) by

$$\delta = \frac{2\pi\rho}{\sqrt{1-\rho^2}}$$

Since the damping ratio is the ratio of actual to critical damping ($\rho=C/C_c$), the actual damping coefficient (labeled C_1 for the wheel) is then determined. The damping coefficient of the wheel was determined to be $C_1=4.0\ lb_f/ft/sec$.

Moments of Inertia. The bifilar pendulum method was used to determine the vehicle moments of inertia about its center of gravity. Since the sprung mass (m_r) is much greater than the unsprung mass (m_u), the moments measured were taken to be the moments of the sprung mass of the vehicle. Plate 4 shows the arrangement used.

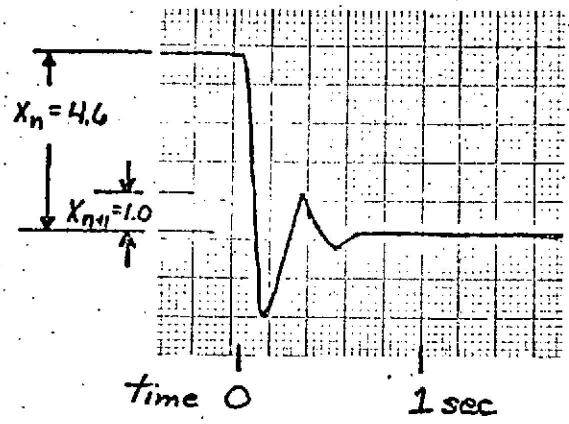

FIGURE 7

Damped Wheel Response

Under 8 Pound Load

Damping Coefficient Calculation:

Critical damping coefficient $C_c = 2m\sqrt{k/m}$ $\quad k_1 = 298$ lb/ft

$m = 8/32.2 \quad lb_m$

$C_c = 17.2$ lb/ft/sec

Logarithmic decrement $\delta = \ln\,(x_n/x_{n+1}) = \ln \frac{4.6}{1.0} = 1.52$

Damping ratio $\zeta = C/C_c$

$$\delta = \frac{2\pi\zeta}{\sqrt{1-\zeta^2}}$$

$$\zeta = 0.232$$

$$c = \zeta c_c = 4.0$$

$$C = 4.0\ lb_f/ft/sec$$

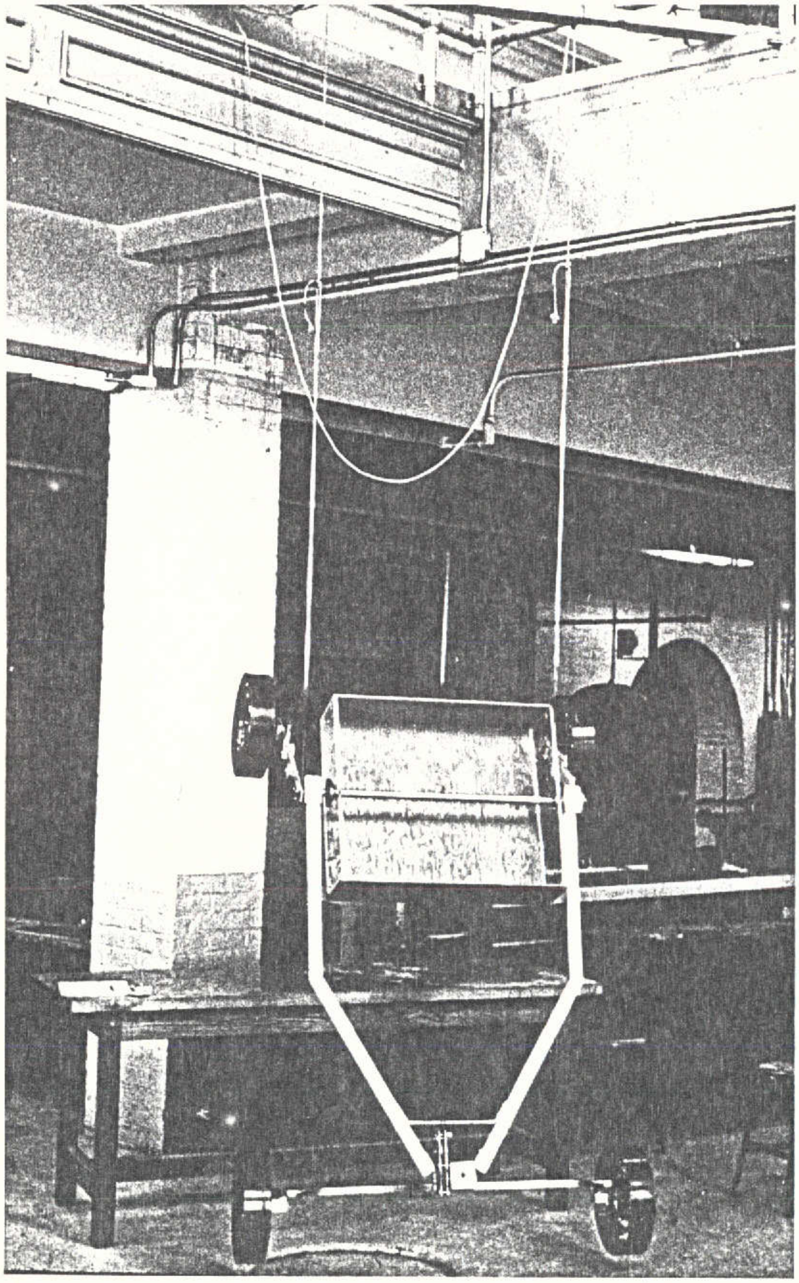

PLATE 4

Bifilar Pendulum Method of Determination

of I_{zz} for the 0.4 RPI-MRV

The commonly used method is basically a torsional pendulum. The vehicle must be suspended so that one of its axes is vertical. Suspended by two identical lines of length L attached to the vehicle at distances R_A and R_B from the c.g. (see Figure 8), the vehicle is displaced angularly in the horizontal plane about the vertical axis through its c.g. A natural torsional pendulum motion results. Once the period of oscillation is determined, the moment of inertia about the vertical axis through the c.g. is determined from

$$I_G = \frac{W R_A R_B t^2}{4\pi^2 L}$$

where w is the total vehicle weight and t is the period of oscillation. This measurement procedure was carried out for all three axes of the primed coordinate system of Figure 2. Plate 2 tabulates the results. The moments of inertia about the unprimed coordinate system of Figure 2 are obtained from the primed axes by use of the parallel axis transfer expression

$$I_{xx} = I_{x'x'} + m_r h^2$$

where h is the distance separating the two axes (Figure 2). These values are also tabulated in Plate 2.

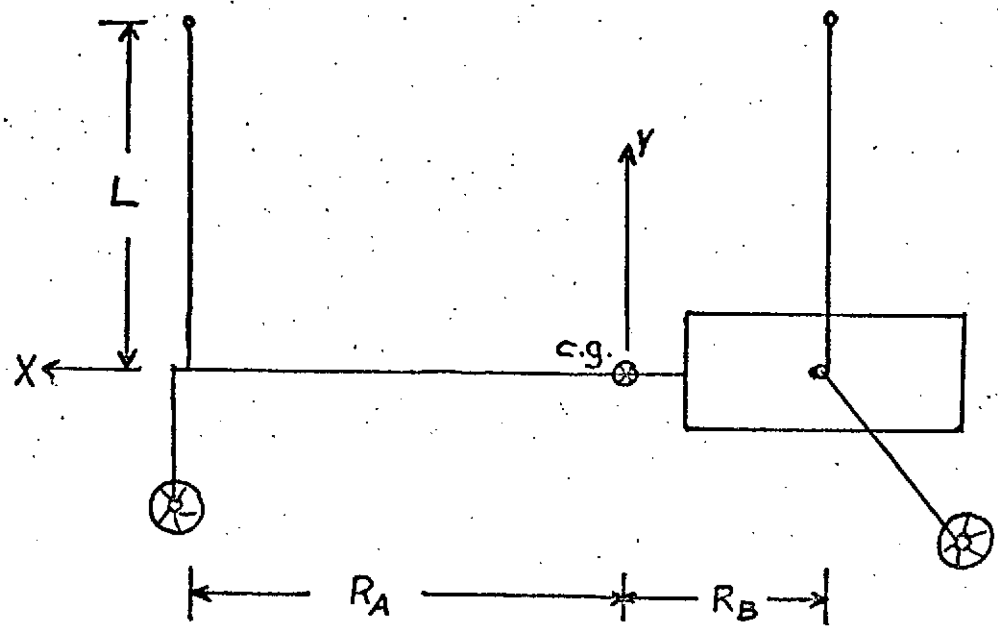

FIGURE 8

Bifilar Pendulum Method for Determining I_{yy}

CHAPTER 4

DYNAMIC TESTING

Approach. The purpose of the dynamic testing was two-fold:

(1) Data was sought for a comparison with the predicted response by the mathematical model

(2) The sources of undesirable motion were located in order to indicate possible corrective alterations.

The dynamic testing proceeded in two directions:

(1) Measurement of transient responses to step input displacements

(2) Measurement of frequency responses to forced constant amplitude sinusoidal displacements

Responses were measured at various vehicle locations as a result of various inputs at different locations. It was then readily apparent that the testing procedure could be simplified. Measurement of the response of the c.g. provided all the necessary information. The procedure is described below.

Equipment. All measurements were made with a capacitance displacement measurement system. Capacitance probes with a maximum range of one inch were used. Plate 5 shows a probe in place for testing. After the signal from the capacitance probe was amplified, it was connected to a strip chart recorder for an output plot. All displacements were calibrated with a dial indicator.

An MB electromagnetic shaker unit was used to provide the sinusoidal forced displacements. The shaker unit was fitted with a

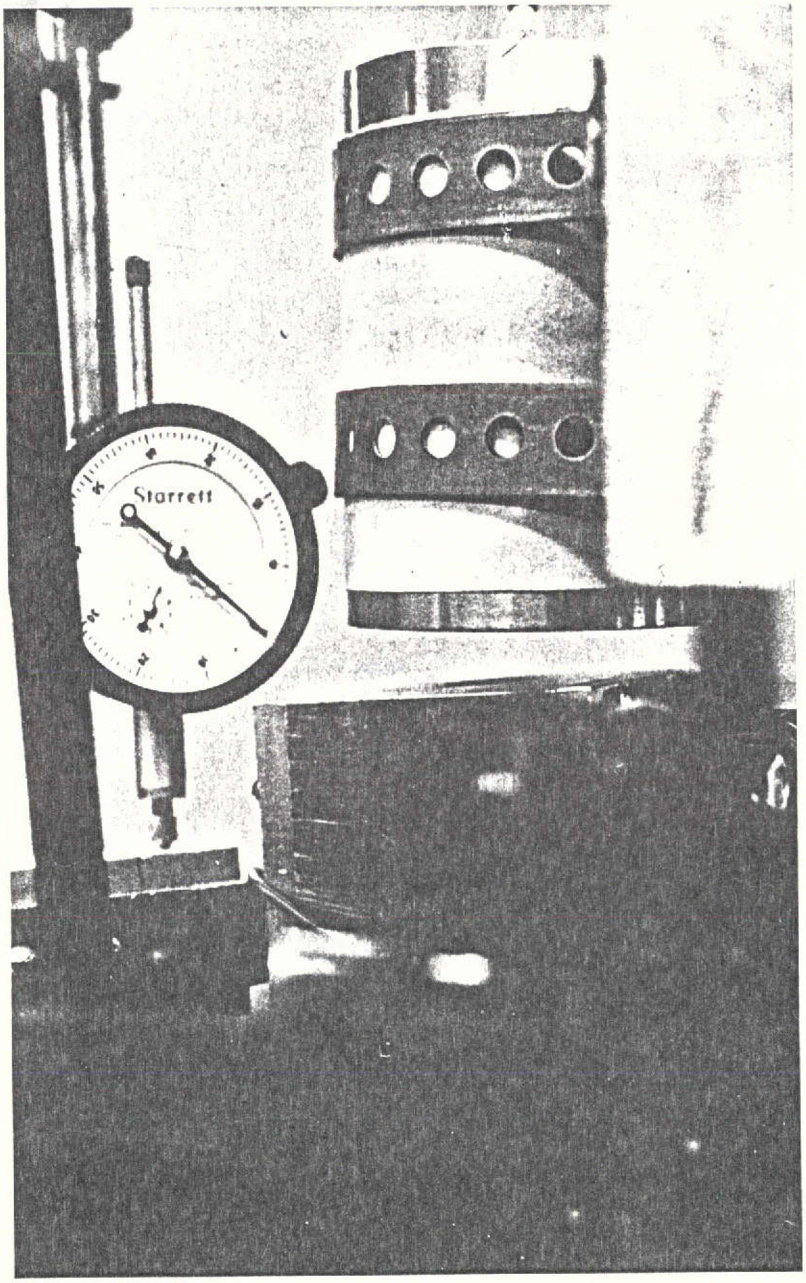

PLATE 5

Close-up View of the

Capacitance Displacement Measuring Probe wood extension arm to provide two platform pads on which the test vehicle was placed (Plate 6). Initially the frequency response of the shaker unit with platform was measured in order to separate the vehicle response from the shaker response. As shown in Figure 9, the shaker unit frequency response is not particularly flat. However, no sharp peaks exist. A comparison of the MRV frequency response (Figure 13) with the shaker unit frequency response shows that the shaker unit caused no gross errors or false peaks.

Testing.

Step Response. The transient response of the c.g. of the MRV to step inputs was measured. Plate 6 shows the general equipment setup for measurement of the vertical response. A close-up view of the capacitance probe and its location relative to a conducting surface on the MRV is shown in Plate 5. The roll and pitch responses were easily determined by the use of two capacitance probes. The two probes were placed on a line parallel to or coinciding with the principal axes of the vehicle. (Plate 7 shows the equipment setup and capacitance probe locations for pitch angle response measurements). For small angles of rotation, the change in angle was simply the difference of the probe readings divided by the distance between the probes. The amplifier used to amplify the signals from the probes was equipped with a difference junction. Therefore the response was easily obtained by connecting the difference junction to the strip chart recorder for a time plot.

All step inputs were simulated by the release of an initial displacement. Using nylon line, a weight was suspended from the desired location on the MRV. The nylon line was then burned to release the

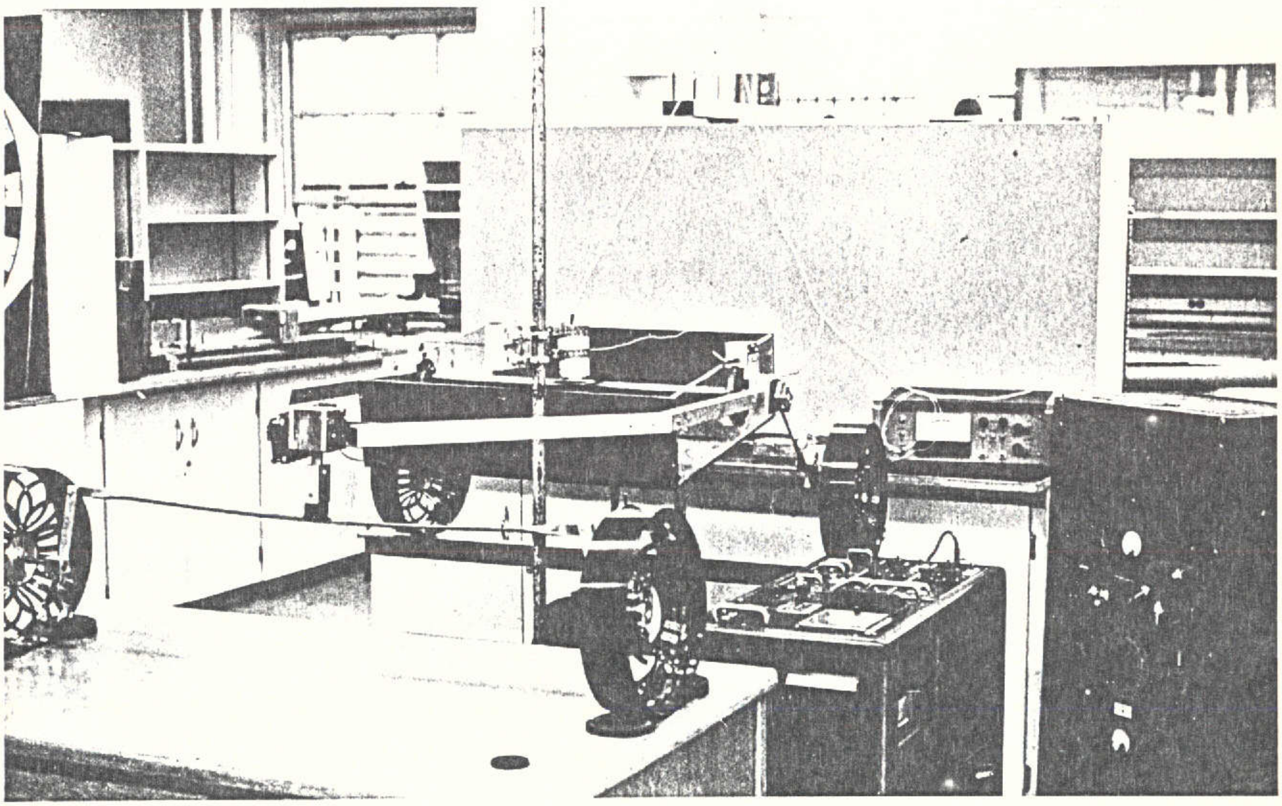

PLATE 6

Equipment Setup for Vertical Displacement

Response Measurement

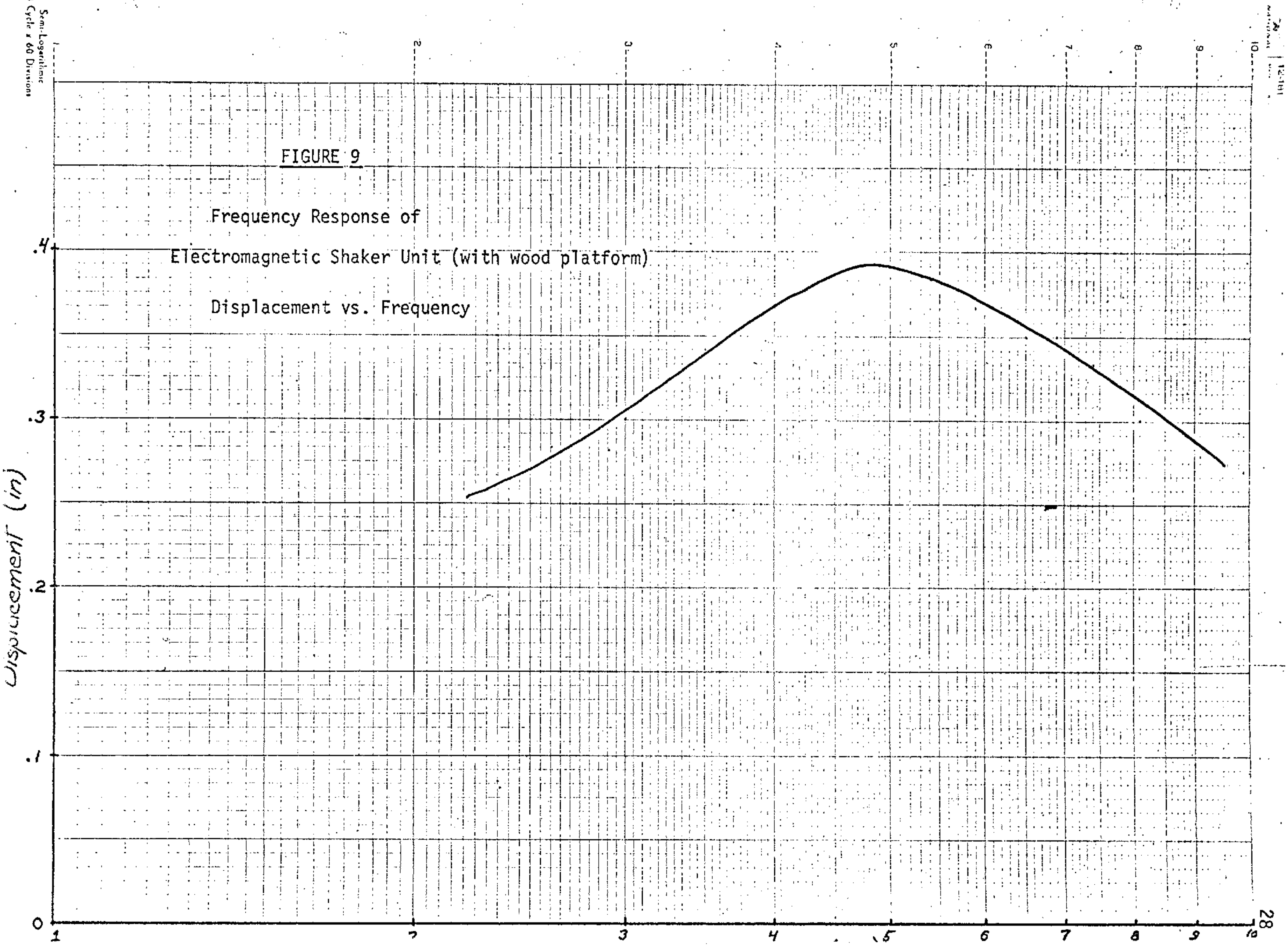

FIGURE 9
Frequency Response of
Electromagnetic Shaker Unit (with wood platform)
Displacement vs. Frequency
Displacement (in)
.4
.3
.2
.1
0
1
2
3
4
5
6
7
8
9
10

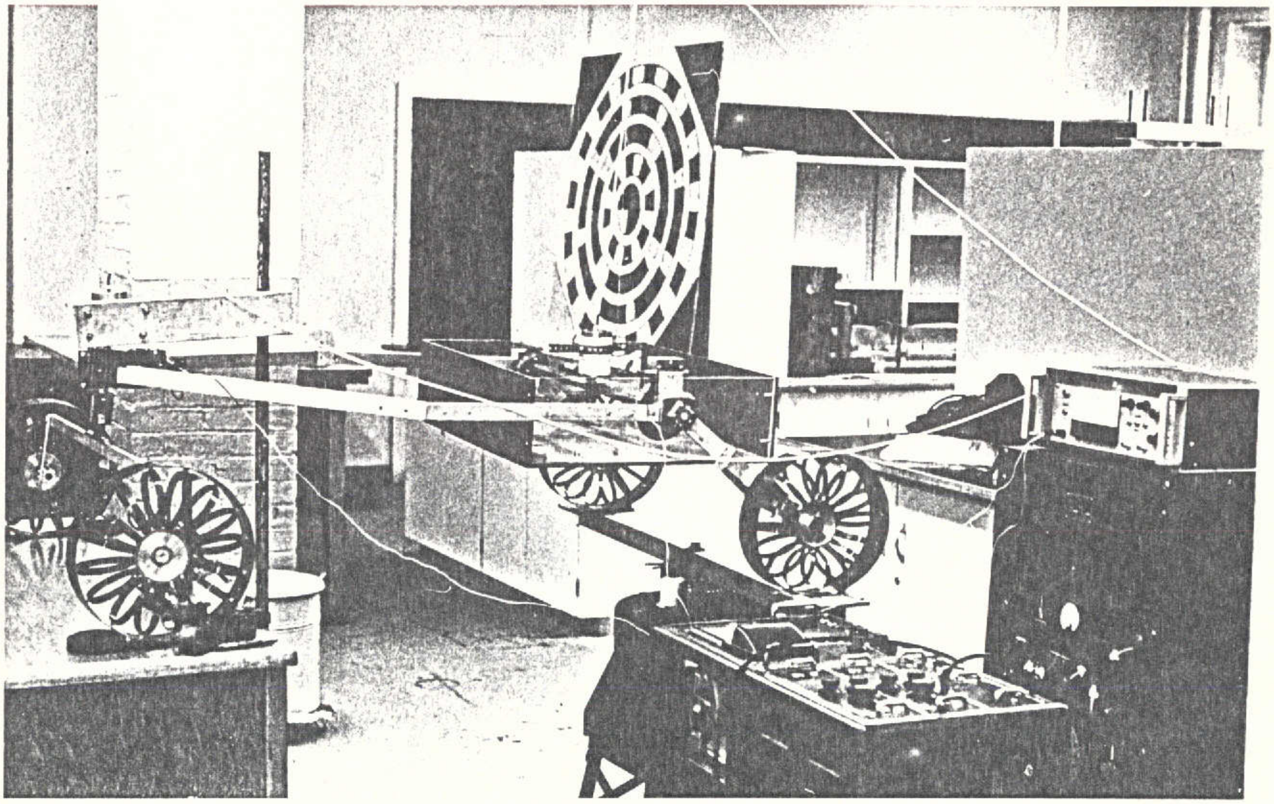

PLATE 7

Equipmemt Setup for Pitch Angle

Response Measurement

weight. Figures 10,11, and 12 show step responses of vertical, pitch, and roll displacements respectively.

Forced frequency response. The MRV may be traversing Martian terrain similar to a washboard surface. Therefore, it is important to determine the natural frequencies which exist in the MRV, and the relative amplitude of vibration at these frequencies. As explained above, the electromagnetic shaker unit was used to force inputs of various frequencies. Since the shaker unit is of too small capacity to vibrate the 0.4 MRV as a whole, the vibration tests were conducted in two phases. Only one set of wheels, front or rear, was driven at one time. Figure 13 shows the frequency response to the sinusoidal inputs to the front and rear wheel pairs. Each curve shows two peaks at the frequencies of about 4.0 cps, and 6.5 cps. The location of the peaks in the response is easily predicted by evaluation of the expressions

$$\omega_n = \sqrt{k/m}, \quad f = \omega_n/2\pi \qquad (17)$$

If the total load on the rear wheels and the equivalent spring constant of the rear wheels ($2k_1$) is substituted into equations (17), the result of f=4.34 cps is obtained. Likewise, if the total front wheel load and spring constant is used, f=6.74 cps. These predicted natural frequencies are reasonably close to the measured frequency response peaks of 4.0 and 6.5 cps. The association of the 4.0 cps peak with the rear wheel pair and the 6.5 peak with the front wheel pair is also a logical conclusion from Figure 13. In the case of the rear wheel pair input curve, the higher peak is associated with a frequency of 4.0 cps, which results from the rear wheel spring. The 6.5 cps peak is similarly associated with the front wheel spring on the front wheel pair input curve.

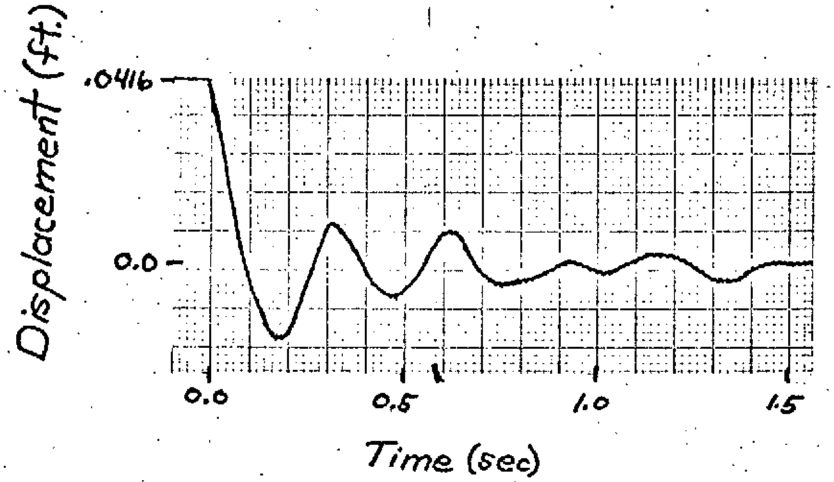

FIGURE 10

Vertical Step Response--Actual

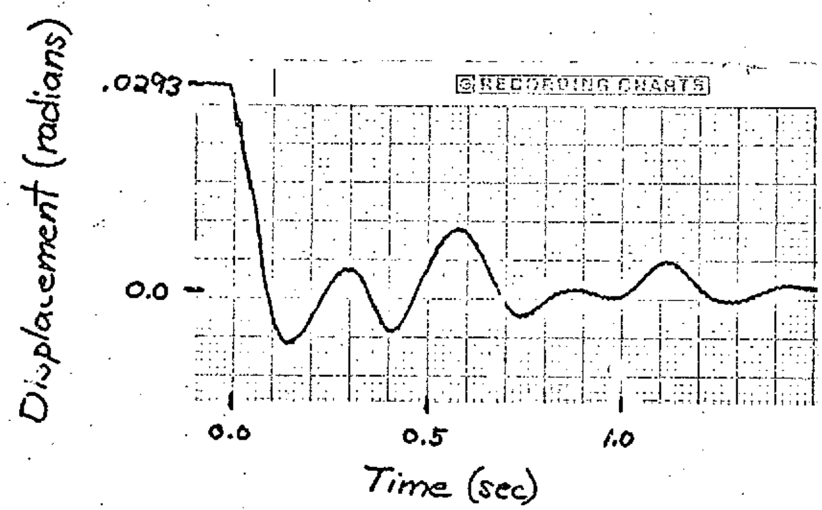

FIGURE 11

Pitch Step Response--Actual

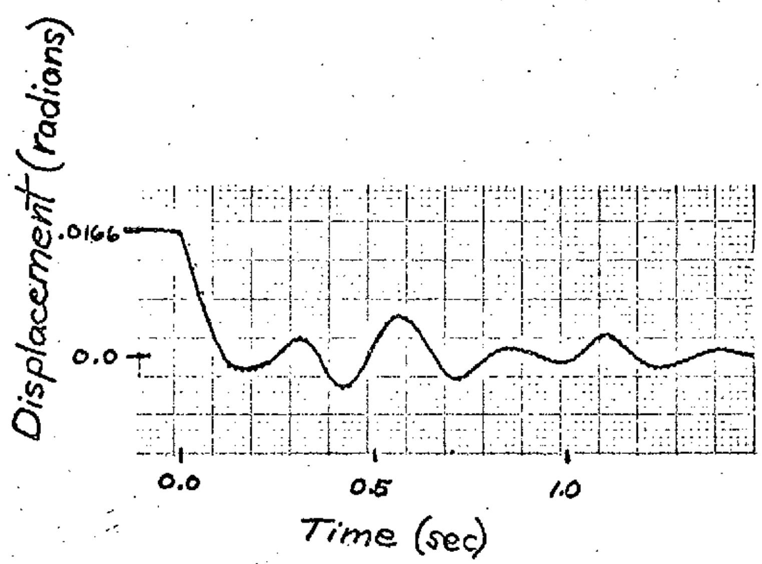

FIGURE 12

Roll Step Response--Actual

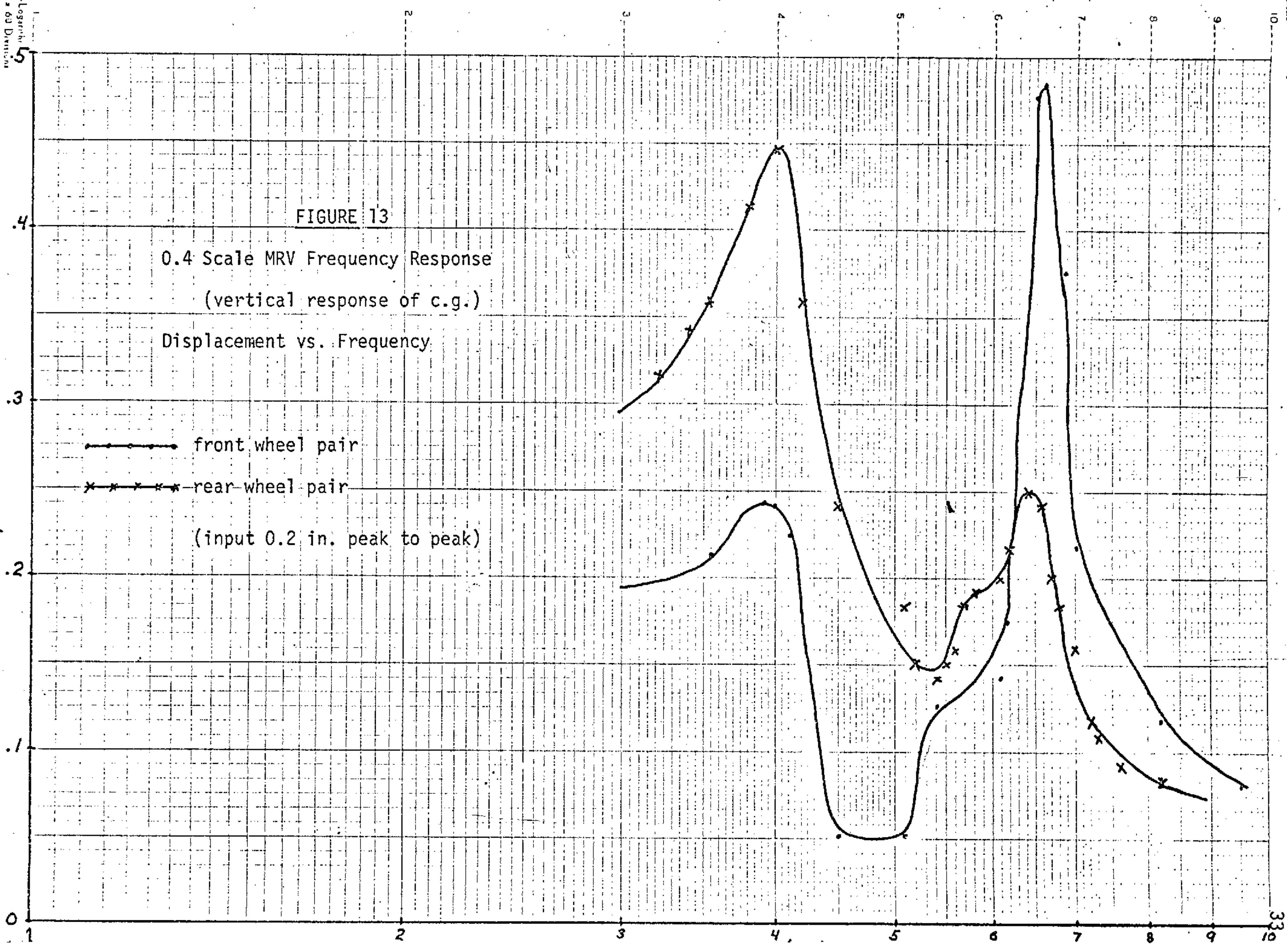

FIGURE 13

0.4 Scale MRV Frequency Response

(vertical response of c.g.)

Displacement vs. Frequency

CHAPTER 5

COMPARISON OF MATHEMATICAL MODEL WITH TEST RESULTS AND CONCLUSIONS

Figures 10, 11, and 12 show actual step input responses of the 0.4 RPI-MRV in the vertical, pitch angle, and roll angle modes, respectively. By setting the initial conditions of the mathematical model equal to the initial conditions imposed upon the physical model, a mathematically predicted response was obtained. Figure 14 shows the predicted vertical response while Figure 15 shows the pitch and roll responses.

A close comparison of the actual response with the predicted response indicates the following:

(a) The period of oscillation of the actual model is about 0.3 seconds in the vertical displacement and pitch response and 0.33 seconds for the roll response. The corresponding values of the predicted response are 0.2 and 0.24 seconds respectively. The mathematical model predicts a somewhat faster response, but correctly predicts an approximate relative difference between the roll response and the vertical/pitch response.

(b) The ratio of the first and second "peak" of the actual vertical response is $x_n/x_{n+1}=4$. The mathematical model predicts less damping showing the same ratio to be $x_n/x_{n+1}=2.1$. However, the general envelop of the actual decaying response shows the oscillation to be reduced to 20% of the initial value after 0.6 seconds. The mathematical model predicts the oscillation envelop to be at about 15% of the initial peak value at the equivalent time. Also

PAGE 3 11/05/73

Y1=Y

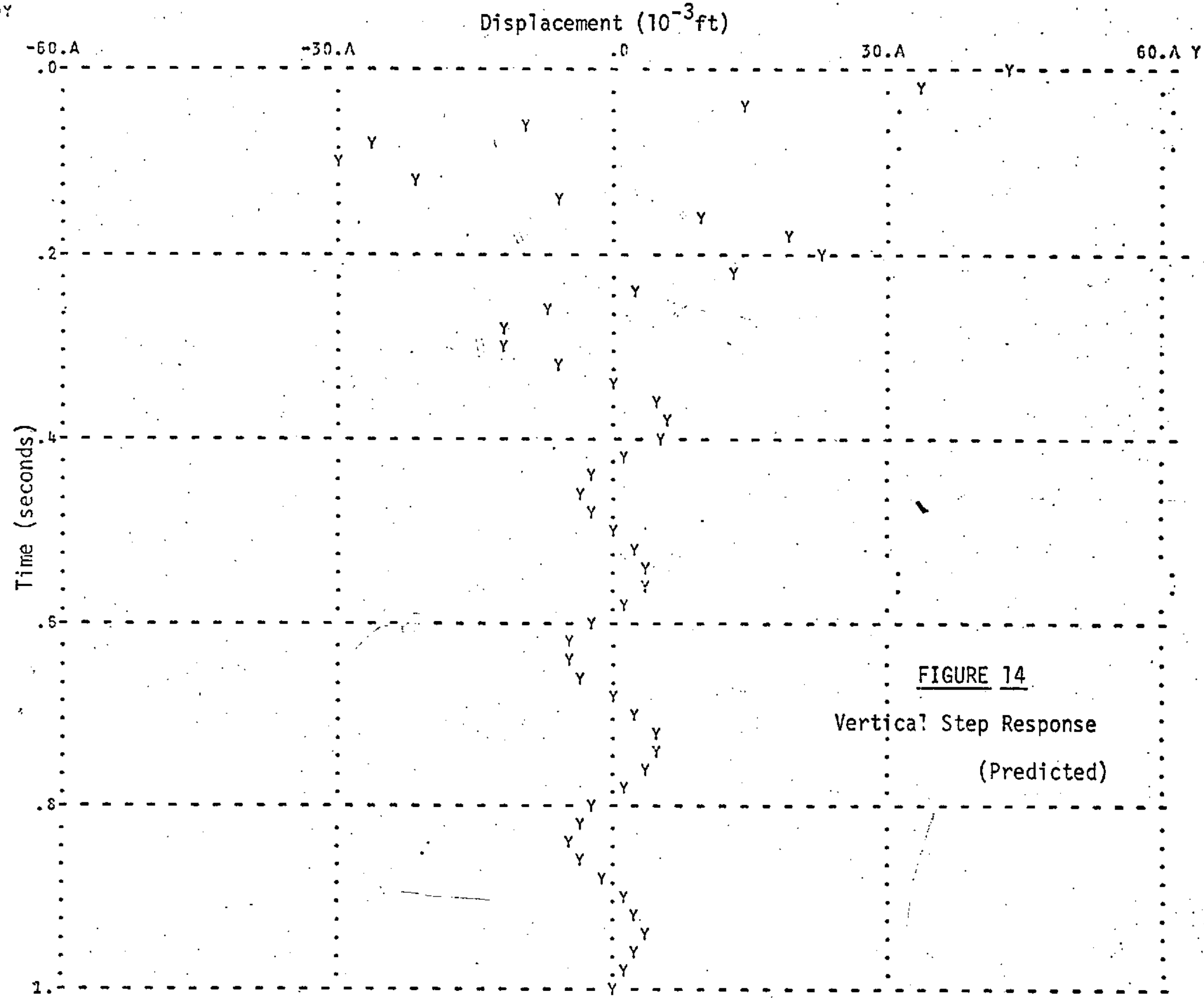

FIGURE 14

Vertical Step Response

(Predicted)

16200 PAGE 4 11/05/73

R1=R,P1=P

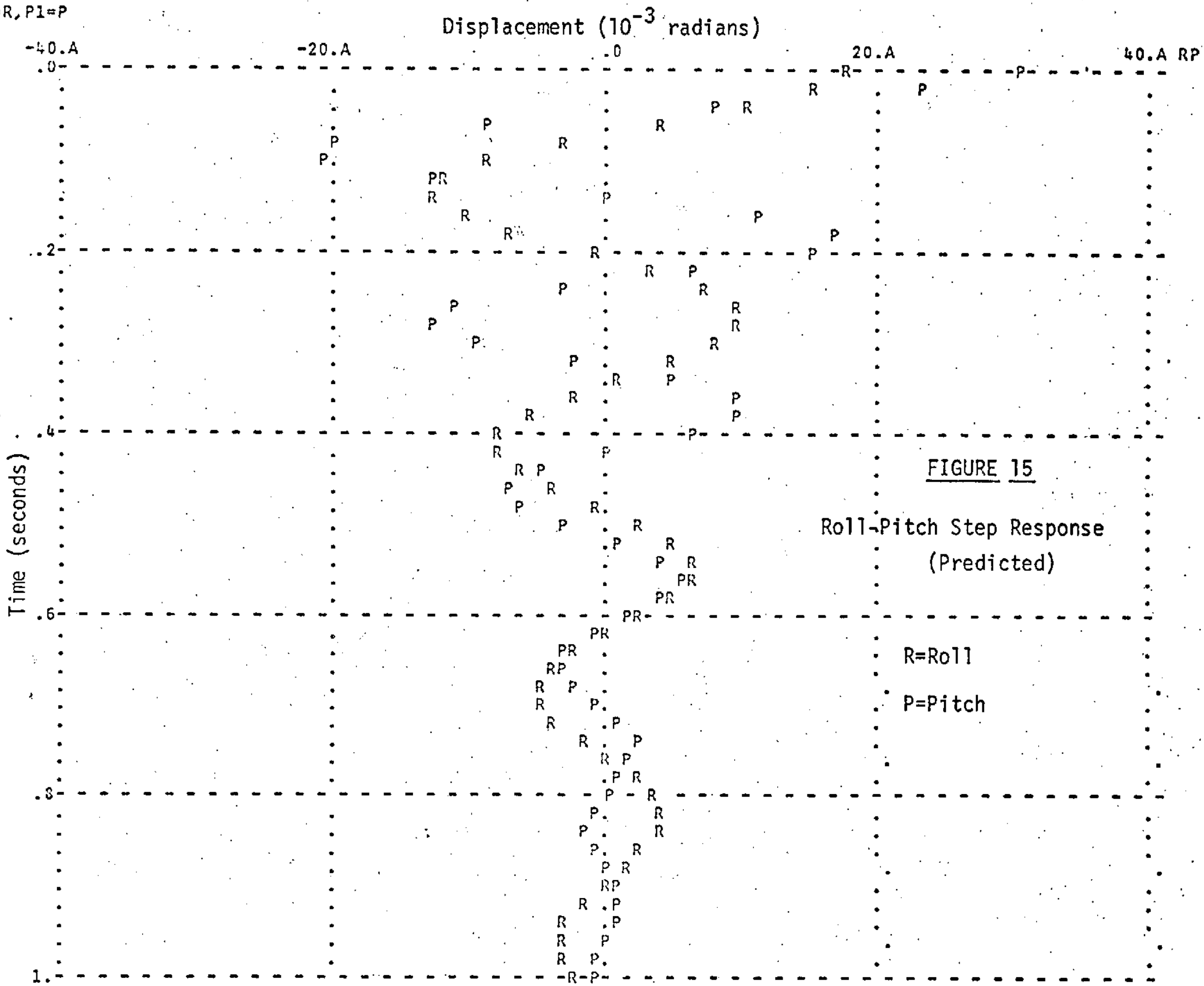

FIGURE 15

Roll-Pitch Step Response (Predicted)

to be noted is the increase in amplitude of oscillation of the actual vertical response between the fourth and fifth peaks in Figure 10. This is due to the transfer of energy from the roll and pitch modes to the vertical mode. The mathematical model correctly predicts the increase in amplitude between the fourth and fifth peaks. A comparison of the actual versus predicted roll and pitch angle responses yields similar results. The general envelop of oscillation is similar in each case. However, the increase in amplitude of the actual response, because of the energy transfer, is not reflected in the predicted response.

Sources of error in the mathematical model are most likely due to the following mathematical deficiencies:

(1) The mathematical model is based on a point mass located at the c.g. of the sprung vehicle. The actual model is quite different with no one general area of mass concentration.

(2) Only three degrees of freedom have been considered in the mathematical model. In reality, the degrees of freedom not considered (lateral and longitudinal horizontal translation and yaw angle displacement) do experience considerable excitation. Since these modes are coupled with the three degrees of freedom considered, there will be considerable energy transfer among all modes. Therefore, neglecting three modes induces considerable error into the mathematical model.

(3) Many of the members of the 0.4 scale model are rather loosely joined. This "slop" is obviously not included in the mathematical model and is therefore a source of error.

An overall evaluation of the mathematical model shows it to be of some value in predicting gross changes in the vehicle response as a result of design parameter changes. For instance, should it be desired to apply a wheel of different spring and damping coefficients, the mathematical model may be used to predict general responses from which comparisons may be made. Likewise, changes in wheel base dimensions or payload location may easily be translated into the mathematical model.

In the optimization of the final vehicle design, a more accurate mathematical model will most likely be desired. The model proposed herein will provide a good basis for extension. Additional degrees of freedom could be included to provide a more sophisticated and more accurate model. For the present time it is felt that this mathematical model will be adequate to help in determining the main design parameters of the 0.4 scale physical working-model, the construction of which is the next step in RPI's vehicle development program.

APPENDIX A

SAMPLE DYNAMO PROGRAM FOR EQUATIONS (15)

11/05/73

```
A
L Y1.K=Y1.J+DT*Y1DOT.JK
R Y1DOT.KL=Y2.K
L Y2.K=Y2.J+DT*Y2DOT.JK
R Y2DOT.KL=A11*Y2.K+A12*Y1.K+B11*R2.K+B12*R1.K+C11*P2.K+C12*P1.K
L R1.K=R1.J+DT*R1DOT.JK
R R1DOT.KL=R2.K
L R2.K=R2.J+DT*R2DOT.JK
R R2DOT.KL=A21*Y2.K+A22*Y1.K+B21*R2.K+B22*R1.K
L P1.K=P1.J+DT*P1DOT.JK
R P1DOT.KL=P2.K
L P2.K=P2.J+DT*P2DOT.JK
R P2DOT.KL=A31*Y2.K+A32*Y1.K+C31*P2.K+C32*P1.K
B
N A11=-4.0*C1/MR
N A12=-4.0*K1/MR
N B11=(L1-L2)*C1/MR
N B12=(L1-L2)*K1/MR
N C11=2.0*(A-B)*C1/MR
N C12=2.0*(A-B)*K1/MR
N A21=(L1-L2)*C1/IXX
N A22=(L1-L2)*K1/IXX
N B21=-(L1*L1+L2*L2)*C1/IXX
N B22=-((L1*L1+L2*L2)*K1/IXX)+(WR*H/IXX)
N A31=(A-B)*2.0*C1/IZZ
N A32=(A-B)*2.0*K1/IZZ
N C31=-(A*A+B*B)*2.0*C1/IZZ
N C32=-((A*A+B*B)*2.0*K1/IZZ)+(WR*H/IZZ)
C
C C1=02.0
C K1=298.0
C MR=1.52
N A=22.25/12.0
N B=34.75/12.0
N L1=21.0/12.0
N L2=23.0/12.0
C IXX=3.73
C IZZ=6.67
C WR=49.0
N H=10.0/12.0
D
N Y1=0.0416
N Y2=0.0
N R1=0.0166
N R2=0.0
N P1=0.0293
N P2=0.0
E
PRINT Y1,R1,P1
PLOT Y1=Y
PLOT R1=R,P1=P
SPEC DT=0.001/LENGTH=01.0/PRTPER=0.02/PLTPER=0.02
RUN
```

Brief Explanation of DYNAMO Program

Statements

A	The set of three second order differential equations (equations (15)) expressed as six first order difference equations in the form required for DYNAMO.
B	The constants of equation (16).
C	The physical characteristics of the 0.4 scale RPI-MRV.
D	The initial conditions.
C	The output statements.

APPENDIX B

ALTERNATE MATHEMATICAL MODEL--1

To increase the damping and to improve the overall vehicle response, it has been proposed to join the MRV frame to the front axle through a spring and damper. Figure 16 shows the schematic diagram for such a configuration. The following is a derivation of the equations of motion for this model.

Inertia Forces. The inertia forces are the same as derived in Chapter 2.

External Forces. From Figure 17, the equivalent rear and front mechanical impedances respectively are:

$$Z_r = 2(k_1 + C_1 s)$$

$$Z_f = \frac{2(k_1 + C_1 s)(k_2 + C_2 s)}{2k_1 + k_2 + (2C_1 + C_2)s} \tag{18}$$

Following the same procedure of virtual displacements as developed previously:

(a) roll with vertical displacement (Figure 3)

$$F_y = -2A_1A_2 y + A_1\theta_x(\ell_1 - \ell_2) - yZ_f \tag{19}$$

$$M_x = yA_1A_2(\ell_1 - \ell_2) - A_1\theta_x(\ell_1^2 + \ell_2^2) + W_r h\theta_x \tag{20}$$

where

$$A_1 = k_1 + C_1 s$$
$$A_2 = Z_2/(Z_1 + Z_2)$$
$$A_3 = 2(k_1 + C_1 s)$$
$$A_4 = (k_2 + C_2 s)$$

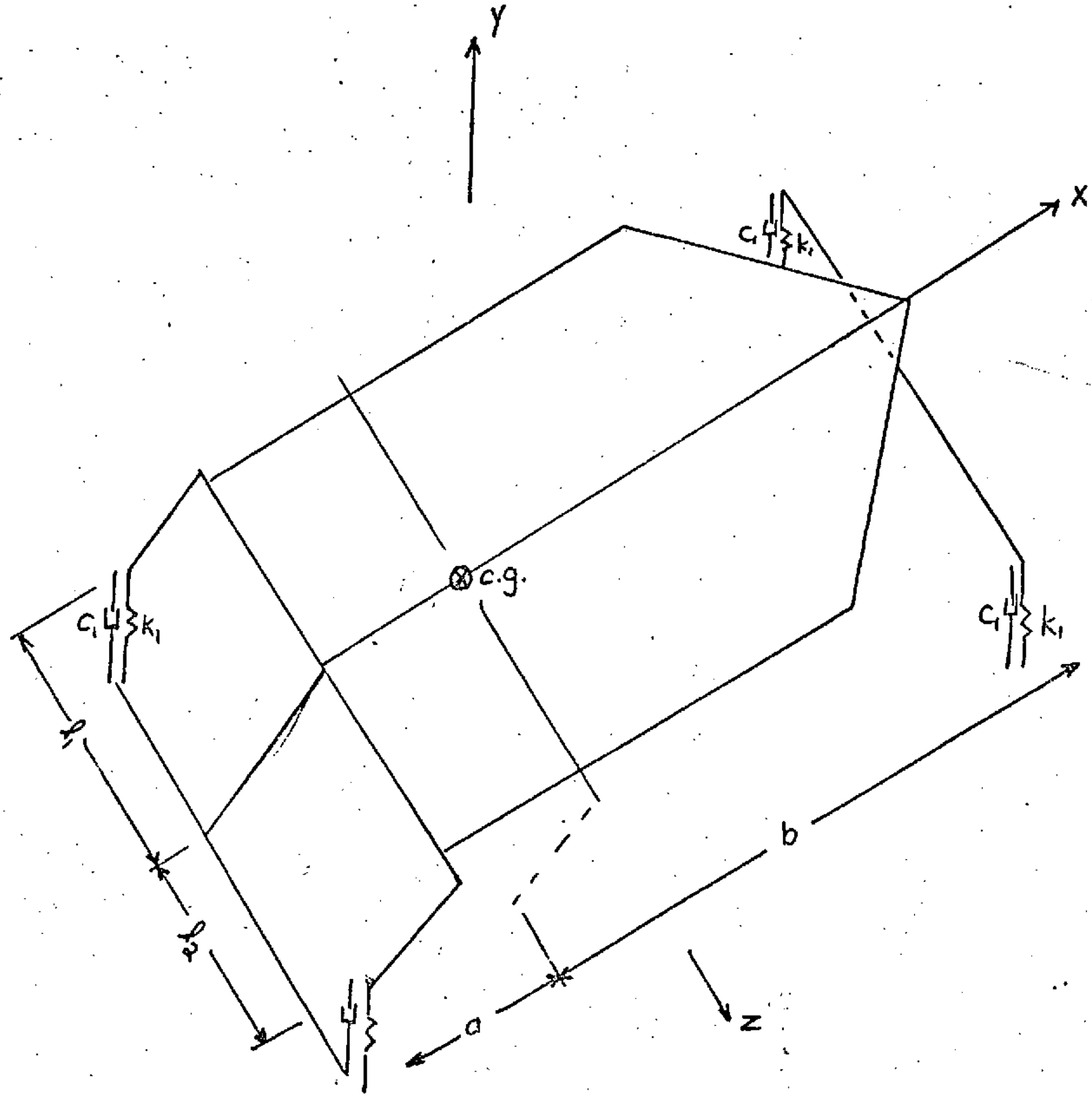

FIGURE 16

RPI-MRV Alternate Model-Schematic

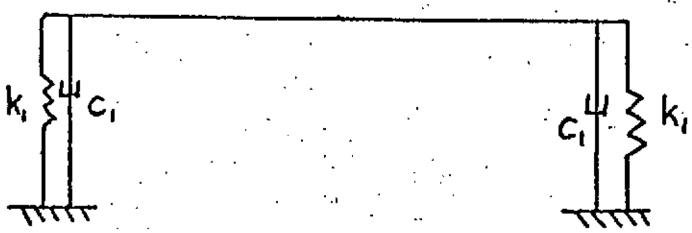

$$Z_r = 2(k_1 + c_1 s)$$

(a) Rear suspension

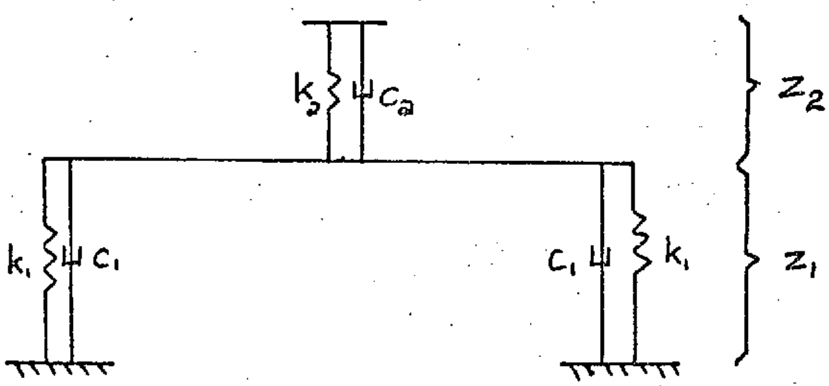

$$Z_f = \frac{1}{\frac{1}{Z_1} + \frac{1}{Z_2}}$$

$$Z_1 = 2(k_1 + c_1 s)$$

$$Z_2 = k_2 + C_2 s$$

$$Z_f = \frac{(2k_1 + 2c_1 s)(k_2 + sC_2)}{2k_1 + k_2 + s(2c_1 + C_2)}$$

(b) Front suspension

FIGURE 17

Alternate Model of RPI-MRV

Front and Rear Suspension

(b) pitch with vertical displacement (Figure 4)

$$F_y = -y(z_r + z_f) + \theta_z(bz_r - az_f) \tag{21}$$

$$M_z = y(bz_r - az_f) + \theta_z(-b^2 z_r - a^2 z_f + hw_r) \tag{22}$$

Combining equations (5), (19), (20), (21), and (22) and simplifying, the equations of motion take the following form:

$$\begin{aligned}
&\dddot{y} + a_{11}\ddot{y} + a_{12}\dot{y} + a_{13}y + b_{11}\ddot{\theta}_x + b_{12}\dot{\theta}_x + b_{13}\theta_x + c_{11}\ddot{\theta}_z + c_{12}\dot{\theta}_z + c_{13}\theta_z = 0\\
&\dddot{\theta}_x + b_{21}\ddot{\theta}_x + b_{22}\dot{\theta}_x + b_{23}\theta_x + a_{21}\ddot{y} + a_{22}\dot{y} + a_{23}y + n_{21}\dot{\theta}_x\dot{\theta}_z + n_{22}\ddot{\theta}_z\dot{\theta}_x + n_{22}\ddot{\theta}_x\theta_z = 0\\
&\dddot{\theta}_z + c_{31}\ddot{\theta}_z + c_{32}\dot{\theta}_z + c_{33}\theta_z + a_{31}\ddot{y} + a_{32}\dot{y} + a_{33}y + n_{31}(\dot{\theta}_x)^2 + n_{32}(\dot{\theta}_x\ddot{\theta}_x) = 0
\end{aligned} \tag{23}$$

where:

$$a_{11} = -\left[\frac{1}{c_2 + 2c_1}\right]\left[(2k_1 + k_2) + \frac{1}{m_r}(4c_1c_2 + 2c_1^2)\right]$$

$$a_{12} = -\left[\frac{1}{c_2 + 2c_1}\right]\left[\left(\frac{4}{m_r}\right)(k_1c_2 + c_1k_2 + c_1k_1)\right]$$

$$a_{13} = -\left[\frac{1}{c_2 + 2c_1}\right]\left[\left(\frac{1}{m_r}\right)(k_1k_2 4 + 2k_1^2)\right]$$

$$b_{11} = +\left[\frac{1}{c_2 + 2c_1}\right]\left[\left(\frac{1}{m_r}\right)c_1(\ell_2 - \ell_1)(c_2 + 2c_1)\right]$$

$$b_{12} = +\left[\frac{1}{c_2 + 2c_1}\right]\left[k_1(c_2 + 2c_1) + c_1(2k_1 + k_2)\right]\left(\frac{1}{m_r}\right)(\ell_2 - \ell_1)$$

$$b_{13} = +\left[\frac{1}{c_2 + 2c_1}\right](\ell_2 - \ell_1)(2k_1^2 + k_1k_2)$$

$$c_{11} = +\left[\frac{1}{c_2 + 2c_1}\right]\left(\frac{1}{m_r}\right)\left[2bc_1^2 + (a - b)c_1c_2\right]$$

$$c_{12} = +\left[\frac{1}{c_2 + 2c_1}\right]\left(\frac{1}{m_r}\right)\left[4c_1bk_1 + (a - b)(c_2k_1 + c_1k_2)\right]$$

$$c_{13} = +\left[\frac{1}{c_2 + 2c_1}\right]\left(\frac{1}{m_r}\right)\left[k_1k_2(a - b) + 2bk_1^2\right]$$

$$a_{21} = +\left[\frac{1}{c_2 + 2c_1}\right]\left(\frac{1}{I_{xx}}\right)(\ell_2 - \ell_1)(c_1c_2)$$

$$a_{22} = +\left[\frac{1}{c_2 + 2c_1}\right]\left(\frac{1}{I_{xx}}\right)(\ell_2 - \ell_1)(k_1c_2 + k_2c_1)$$

$$a_{23} = +\left[\frac{1}{c_2 + 2c_1}\right]\left(\frac{1}{I_{xx}}\right)(\ell_2 - \ell_1)(k_1k_2)$$

$$b_{21} = +\left[\frac{1}{c_2 + 2c_1}\right]\left[(2k_1 + k_2) + \frac{1}{I_{xx}}(\ell_1^2 + \ell_2^2)(c_1c_2 + 2c_1^2)\right]$$

$$b_{22} = +\left[\frac{1}{c_2 + 2c_1}\right]\left(\frac{1}{I_{xx}}\right)\left\{(\ell_1^2 + \ell_2^2)\left[c_1(2k_1 + k_2) + k_1(c_2 + 2c_1)\right] - w_r h(2c_1 + c_2)\right\}$$

$$b_{23} = +\left[\frac{1}{C_2+2C_1}\right]\left(\frac{1}{I_{xx}}\right)\left[(\ell_1^2+\ell_2^2)k_1(2k_1+k_2) - W_r h(2k_1+k_2)\right]$$

$$a_{31} = +\left[\frac{1}{C_2+2C_1}\right]\left(\frac{1}{I_{zz}}\right)\left[4bc_1^2 + c_1c_2 2(b-a)\right]$$

$$a_{32} = +\left[\frac{1}{C_2+2C_1}\right]\left(\frac{1}{I_{zz}}\right)\left[8bc_1k_1 + 2(b-a)(c_1k_2+c_2k_1)\right]$$

$$a_{33} = +\left[\frac{1}{C_2+2C_1}\right]\left(\frac{1}{I_{zz}}\right)\left[4bk_1^2 + 2k_1k_2(b-a)\right]$$

$$c_{31} = +\left[\frac{1}{C_2+2C_1}\right]\left\{(2k_1+k_2) + \frac{1}{I_{zz}}\left[b(a^2+b)(4c_1^2+2c_1+c_2)\right]\right\}$$

$$c_{32} = +\left[\frac{1}{C_2+2C_1}\right]\left(\frac{1}{I_{zz}}\right)\left[2b(a^2+b)(4c_1k_1+c_1k_2+c_2k_1) - W_r h(2c_1+c_2)\right]$$

$$c_{33} = +\left[\frac{1}{C_2+2C_1}\right]\left(\frac{1}{I_{zz}}\right)\left[4a^2bk_1^2 + 2a^2bk_1k_2 + 4bk_1^2 + 2b^2k_1k_2 - W_r h(2k_1+k_2)\right]$$

$$n_{21} = -\left[\frac{1}{C_2+2C_1}\right]\left(\frac{I_{xy}}{I_{xx}}\right)(2k_1+k_2)$$

$$n_{22} = -I_{xy}/I_{xx}$$

$$n_{31} = \left[\frac{1}{C_2+2C_1}\right]\left(-I_{xy}/I_{zz}\right)(2k_1+k_2)$$

$$n_{32} = -2I_{xy}/I_{zz}$$

The digital computer program DYNAMO is an excellent method to use to solve equations (23).

Initially one would believe that the simpler mathematical model developed for the schematic of Figure 1 could be obtained from equations (23) merely by letting the values of C_2 and k_2 approach infinity. A look at the coefficient terms shows that no meaningful expressions result if this limit is taken. An alternate way to negate the effects of C_2 and k_2 would be to equate them to high values in the solution of equations (23) with the DYNAMO program.

Although this solution would yield desired results, it would be impractical. Large values of k and C associated with relatively small values of m in mechanical systems yield high time constants (time constant $T \propto 1/\sqrt{k/m}$). Any method of solution of differential equations depends upon a sufficiently small step (time interval in this case) to yield reasonably accurate results. A smaller step size necessitates a larger number of iterations in the calculations to span a specified time interval. This results in considerable more computer time. Therefore, equations (23) should not be used in order to model the simplified schematic of Figure 1.

APPENDIX C

ALTERNATE MATHEMATICAL MODEL--2

Because of limitations at the time of construction of the 0.4 scale MRV, all four toroidal wheels have identical physical properties. The mathematical model developed in the main text of this report is based upon this existing model.

Since the vehicle configuration is designed so that the rear wheel pair supports 70-80% of the total vehicle weight, the stiffness and damping coefficient of the rear wheel should be proportionally greater than the front wheel properties. This appendix presents a mathematical model where the physical characteristics of the wheels are not identical. The subscript 'f' denotes front while the subscript 'r' denotes rear.

The inertia forces of equation (5) remain the same. The external forces due to displacement in the vertical and roll mode are rewritten from equations (6) and (7) as follows:

$$F_y = -(k_r + C_r s)(y - \ell_1\Theta_x) - (k_r + C_r s)(y + \ell_2\Theta_x) - 2(k_f + C_f s) \tag{24}$$

$$M_x = (\ell_1 - h\Theta_x)(k_r + C_r s)(y - \ell_1\Theta_x) - (\ell_2 + h\Theta_x)(k_r + C_r s)(y + \ell_2\Theta_x) + W_r(h - y)\Theta_x \tag{25}$$

Using the small displacement approximations, $\ell_1 >> h\Theta_x$, $\ell_2 >> h\Theta_x$, and $h >> y$, equations (24) and (25) become

$$F_y = -(k_r + C_r s)[(y - \ell_1\Theta_x) + (y + \ell_2\Theta_x)] - 2(k_f + C_f s)y \tag{26}$$

$$M_x = (k_r + C_r s)[y(\ell_1 - \ell_2) - \Theta_x(\ell_1^2 + \ell_2^2)] + W_r h\Theta_x \tag{27}$$

Similarly the resultant external forces due to a displacement in the vertical and pitch mode follow from equations (10) and (11):

$$F_y = -2(k_r + sC_r)(y - a\theta_z) - 2(k_f + C_f s)(y + b\theta_z) \tag{28}$$

$$M_z = 2(k_r + C_r s)(a - h\theta_z)(y - a\theta_z) - 2(k_f + C_f s)(b + h\theta_z)(y + b\theta_z) + W_r(h - y)\theta_z \tag{29}$$

Again with the small angle approximations these equations reduce to

$$F_y = -2[(k_r + C_r s)(y - a\theta_z) + (k_f + C_f s)(y + b\theta_z)] \tag{30}$$

$$M_z = 2a(k_r + C_r s)(y - a\theta_z) - 2b(k_f + C_f s)(y + b\theta_z) + W_r h\theta_z \tag{31}$$

Combining equations (5), (26), (27), (30), and (31), and rearranging, the final form results:

$$\ddot{y} + a_{11}\dot{y} + a_{12}y + b_{11}\dot{\theta}_x + b_{12}\theta_x + c_{11}\dot{\theta}_z + c_{12}\theta_z = 0$$

$$\ddot{\theta}_x + b_{21}\dot{\theta}_x + b_{22}\theta_x + a_{21}\dot{y} + a_{22}y = 0$$

$$\ddot{\theta}_z + c_{31}\dot{\theta}_z + c_{32}\theta_z + a_{31}\dot{y} + a_{32}y = 0$$

where

$a_{11} = -\frac{2}{m_r}(c_r + c_f)$

$a_{12} = -\frac{2}{m_r}(k_r + k_f)$

$b_{11} = (\ell_2 - \ell_1)c_r/m_r$

$b_{12} = (\ell_2 - \ell_1)k_r/m_r$

$c_{11} = 2(a-b)c_r/m_r$

$c_{12} = 2(a-b)k_r/m_r$

$b_{21} = (\ell_1^2 + \ell_2^2)c_r/I_{xx}$

$b_{22} = (\ell_1^2 + \ell_2^2)k_r/I_{xx} - W_r h/I_{xx}$

$a_{21} = (\ell_2 - \ell_1)c_r/I_{xx}$

$a_{22} = (\ell_2 - \ell_1)k_r/I_{xx}$

$c_{31} = \frac{2}{I_{zz}}(a^2 c_r + b^2 c_f)$

$c_{32} = \frac{2}{I_{zz}}(a^2 k_r + b^2 k_f - \frac{1}{2}W_r h)$

$a_{31} = \frac{2}{I_{zz}}(bc_r - ac_f)$

$a_{32} = \frac{2}{I_{zz}}(bk_r - ak_f)$

k_r=spring rate of rear wheel

k_f=spring rate of front wheel

C_r=damping coefficient of rear wheel

C_f=damping coefficient of front wheel

a,b,ℓ_1,ℓ_2,h, refer to the dimensions of Figure 1

m_r,w_r,I_{xx},I_{zz} refer to vehicle physical characteristics of Plate 2

REFERENCES

1. Segal, Leonard, "Theoretical Prediction and Experimental Substantiation of the Response of the Automobile to Steering Control", Institution of Mechanical Engineers, Proceedings of the Automobile Division, 1956-57, pages 310-330
2. Timoshenko, S., and Young, D.H., Vibration Problems in Engineering, D. Van Nostrand Company, Inc., 1955
3. Shigley, J.E., Theory of Machines, McGraw-Hill Book Company, 1961
4. Pugh, A., DYNAMO II User's Manual, MIT Press, 1970
5. Cobb, W.A., "Dynamic Evaluation of a Scaled 4 Wheel Martian Roving Vehicle", Master's Project Report, Rensselaer Polytechnic Institute, Troy, New York, June 1972